

Non-Equilibrium Skewness, Market Crises, and Option Pricing: Non-Linear Langevin Model of Markets with Supersymmetry

Igor Halperin¹

July 5, 2022

Abstract:

This paper presents a tractable model of non-linear dynamics of market returns using a Langevin approach. Due to non-linearity of an interaction potential, the model admits regimes of both small and large return fluctuations. Langevin dynamics are mapped onto an equivalent quantum mechanical (QM) system. Borrowing ideas from supersymmetric quantum mechanics (SUSY QM), we use a parameterized ground state wave function (WF) of this QM system as a direct input to the model, which also fixes a non-linear Langevin potential. A stationary distribution of the original Langevin model is given by the square of this WF, and thus is also a direct input to the model. Using a two-component Gaussian mixture as a ground state WF with an asymmetric double well potential produces a tractable low-parametric model with interpretable parameters, referred to as the NES (Non-Equilibrium Skew) model. Supersymmetry (SUSY) is then used to find time-dependent solutions of the model in an analytically tractable way. The model produces time-varying variance, skewness and kurtosis of market returns, whose time variability can be linked to probabilities of crisis-like events. For option pricing out of equilibrium, the NES model offers a closed-form approximation by a mixture of three Black-Scholes prices, which can be calibrated to index options data and used to predict moments of future returns. The NES model is shown to be able to describe both regimes of a benign market and a market in a crisis or a severe distress.

¹Fidelity Investments. E-mail: igor.halperin@fmr.com. Opinions expressed here are author's own, and do not represent views of his employer. A standard disclaimer applies. E-mail for communications on the paper: ighalp@gmail.com

I would like to thank Damiano Brigo, John Dance, Cris Doloc and Lisa Huang for comments and helpful remarks.

1 Introduction

This paper presents an analytically tractable model of non-linear dynamics of market returns using a Langevin approach, with five free parameters. Market returns are driven by a combination of a non-linear potential (a function of returns) controlled by four parameters $\mu, \sigma_1, \sigma_2, a$, and a Gaussian white noise, whose strength gives a fifth parameter h .² Due to a non-linear potential, the model admits regimes of both small and large return fluctuations. A stationary distribution of the model is given by a function that only involves the first four parameters $\mu, \sigma_1, \sigma_2, a$, while parameter h controls *time-dependent* effects. Both the stationary distribution and a time-dependent transition probability density are analytically tractable and available in closed form or in quadratures. The model produces closed-form approximations for option pricing and market crash or crises probabilities. *Mutatis mudandis*, the model can also be applied to individual stocks, though this direction is not pursued further in this paper.

The return distribution obtained with the model can be represented as a sum of a stationary distribution and a time-varying component. The stationary distribution is a *direct input* to the model, in contrast to more traditional approaches where a stationary distribution is normally an output, rather than an input to a model. In this paper, the stationary distribution is given by the square of a two-component Gaussian mixture (which produces a *three*-component Gaussian mixture), defined using four parameters $\mu, \sigma_1, \sigma_2, a$. When these parameters are kept constant, this distribution defines a fully stationary (and possibly not reachable in practice) regime of a financial market. A more realistic assumption could be to have these parameters slowly varying in time, e.g. in an accord with stages of a business cycle.

While a stationary return distribution is an *input* to our model, the *output* is given by a time-varying, dynamic component of the return distribution obtained with the model. The dynamic component is driven by *both* the first four parameters $\mu, \sigma_1, \sigma_2, a$ and the fifth parameter h . The latter controls probabilities of large market drops or crises within a certain time horizon, e.g. a year, and hence drives the market skewness (and other moments) in a non-equilibrium setting. We will therefore refer to the model presented below as the Non-Equilibrium Skew (NES) model. The NES model can be calibrated in a number of ways. For example, if parameters $\mu, \sigma_1, \sigma_2, a$ are kept fixed, parameter h can be calibrated on the fly to market quotes on deep out-of-the money options on the S&P500 index (SPY options), or market spreads on credit default indices such as CDX or iTraXX. Alternatively, *all* model parameters can be calibrated to multiple options with varying strikes or/and maturities. The inferred parameter h controls time-dependent corrections to the stationary distribution, as well as the speed of a relaxation to the stationary distribution.

A decomposition of the return distribution into a stationary and a time-varying component is very convenient because it allows one, among other things, to also decompose moments of the distribution such as variance or skewness into a constant and time-varying components. While substantial time variations of moments of return distributions in financial markets are well documented phenomena, models that try to fit or explain such variations usually do not introduce such a structural separation. Instead, they follow purely statistical or CAPM-based regression-based approaches (see e.g. [19]), or use option pricing models to try to infer market views on future variance or skewness from option quotes, see e.g. [30]. Option-based approaches usually infer moments of a risk-neutral (option-price implied) return distribution rather than a real return distribution, and additional modeling steps are required to relate the two distributions.

The model presented in this paper constructs a direct link between deep out-of-the-money (OTM) options, or alternatively credit indices such as CDX or iTraXX, and future moments of returns. By translating the latter type of market data into market-implied probabilities of large market drops or market crises, the model can be calibrated to such implied probabilities, and then translate them into a weight of a time-varying component of the skew (or variance), and its value versus a time-independent component

²Anecdotal evidence suggests that models with four or five parameters are often able to capture even very complex dynamic systems [35].

resulting from the stationary distribution. The empirical finance literature established contemporaneous correlations between a state of economy (e.g. proxied by the S&P 500 returns) and the returns' skewness, as well as explored ways to use the historical or option-implied market skewness or variance as predictors of future returns, see e.g. [14, 30]. This paper offers a theoretical framework to pursue both sorts of analysis, with a clear separation between a static and dynamic components of the problem.

The NES model produces analytical approximations for option pricing in a non-equilibrium setting, thus enabling using option data to estimate future time-varying moments of returns. Remarkably, the end result of the NES model as applied to option pricing is a *mixture of three Black-Scholes prices*, where all parameters are fixed in terms of the original model parameters $\mu, \sigma_1, \sigma_2, a, h$. Numerical experiments show that the model is flexible enough to both calibrate to option data and match typical levels of market volatility and skewness across different market regimes.

The model developed here is based on a Langevin approach where we directly model non-linear stochastic dynamics of market log-returns, denoted y_t in this paper. With the Langevin approach, dynamics are defined in terms of an interaction potential function $V(y_t)$ and a noise term. For the latter, we use a simplest assumption of a constant Gaussian noise, though other more complex specifications (e.g. a state-dependent Gaussian noise, a non-Gaussian noise, or various multivariate extensions) could also be considered. For the former, we choose a potential function $V(y)$ for which a stationary distribution $p_s(y_t)$ of log-returns has a known and *fixed* functional form, and is given by a three-component Gaussian mixture mentioned above. In other words, a potential $V(y)$ in this paper is constructed in such a way that the problem becomes *quasi-exactly solvable*. Here the word 'quasi' refers to the fact that while the stationary distribution $p_s(y_t)$ is an analytical expression, and is actually an input to our model, the model output amounts to computing the *dynamic* behavior - and this requires some computational efforts, and relies on certain approximations.

To develop an analytically tractable formulation, with easily computable approximations that could also be improved to any required precision, we borrow ideas from physics. First, we use a hidden supersymmetry of Langevin dynamics that was discovered in the 1980s [13]. The Langevin dynamics are mapped onto an equivalent quantum mechanical (QM) system, where the role of the Planck constant \hbar is played by the square of the volatility parameter h^2 (which explains our choice for this variable). In such an equivalent QM system, the hidden supersymmetry (SUSY) of the original Langevin dynamics becomes manifest, see e.g. [21]. The resulting equivalent QM system is mathematically identical to an Euclidean version of supersymmetric quantum mechanics (SUSY QM) developed by Witten [34] in 1981. While SUSY QM was originally proposed as a toy model to study supersymmetry in quantum field theory and string theory, since then it has become a topic of research on its own. In particular, researchers in SUSY QM found that SUSY can be used to develop very efficient computational schemes for computing wave functions or energies of different QM systems, that are often both simpler and more efficient than more traditional methods of computing in quantum mechanics, see e.g. [8] or [21]. This paper proposes to use this machinery to model non-linear stochastic dynamics of market returns.

Further using ideas from SUSY QM [8], we use a parameterized ground state wave function (WF) of this QM system as a *direct input* to the model, which also fixes a non-linear Langevin potential $V(y)$. A stationary distribution of the original Langevin model is given by the square of this WF, and thus is also a direct input to the model. This ensures that the model is quasi-exactly solvable. We use a two-component Gaussian mixture with parameters $\mu, \sigma_1, \sigma_2, a$ as a model of a ground state WF with an asymmetric double well potential, one of the most canonical examples in physics [23, 36]. This parametrization produces a tractable low-parametric model with intuitive and interpretable parameters, where supersymmetry (SUSY) is used to find time-dependent solutions of the model in an analytically tractable way.

Note that while a Langevin model with a non-linear potential could be introduced based on phenomenological grounds, the approach of this paper is motivated by previous work in [16] and [17] that

developed a non-linear Langevin model of stock price dynamics. A model developed in [16, 17], called the QED ("Quantum Equilibrium-Disequilibrium") model, explains non-linearities of price dynamics as a combined effect of capital inflows or outflows in the market, and their impact on asset returns, modeled as a linear or quadratic function of capital inflows. In [18], the single-stock QED model is generalized to an interacting multi-asset universe composed of N risky assets, and re-formulated in terms of returns rather than prices. This results in Langevin dynamics in the return space with a quartic non-linearity of a Langevin potential.³ The approach of [16, 17, 18] provides a theoretical motivation for considering non-linear Langevin dynamics, however here the potential function has the same properties, but is chosen somewhat differently to improve tractability of a resulting model. More specifically, the potential used in this paper is 'semi-phenomenological', and is inspired by a double-well potential, one of the most famous potentials in quantum and statistical mechanics and quantum field theory, that serves there as a prime model for describing quantum tunneling and thermally induced barrier transitions [23, 36].⁴

Theoretical links notwithstanding, non-linear Langevin models for market returns can also be considered on purely phenomenological grounds. Note that squares of market returns are sometimes used in the literature as additional cross-sectional predictors of stock returns in quadratic extensions of the CAPM model [29], also referred to as 'quadratic CAPM' models, see e.g. [6] and references therein.

In this paper, squares and higher powers of market returns are used for time-series modeling. The main novelty of our Non-Equilibrium Skew (NES) model is that non-linearities of return *dynamics* give rise to certain solutions that are simply impossible to obtain starting with a linear model, or even with a non-linear model but treated using methods of perturbation theory. Other, *non-perturbative* (i.e. not traceable within a perturbation theory) saddle-point solutions of the dynamics called *instantons* become important to capture the right dynamics of the model. While instantons are encountered in many problems in statistical physics and quantum field theory (see e.g. [36]), the QED model of [16, 17, 18] suggest that instantons might also be relevant for modeling of market prices and returns. This paper offers further insights into the importance of instantons (and, in general, of a non-linear and non-perturbative analysis) for modeling dynamics producing both small and large market fluctuations - with the latter interpreted as events of a severe market downturn or a crisis. More specifically, instantons and other non-linear effects induce both market crises and market skewness, enabling a theoretical link between them.

The paper is organized as follows. Sect. 2 presents the Langevin model along with its Fokker-Plank and Schrödinger representations that produce an equivalent quantum mechanical (QM) system. Sect. 2.2 introduces supersymmetry (SUSY) as a tool to solve the QM system, and Sect. 2.3 presents a quasi-exactly solvable NES model for a Langevin potential motivated by a double well potential in QM. Instantons and their role in dynamics are discussed in Sect. 2.4. Sect. 3 applies SUSY to compute pre-asymptotic corrections to a stationary distribution of the model. Sect. 4 presents a simplified practical implementation of the NES model, and then applies it to explore time variations in return moments, and to option pricing out of equilibrium. Sect. 4.2 shows that pricing of European options in the NES model reduces to a three-component mixture of Black-Scholes option prices, where all parameters are fixed in terms of the original model parameters. All non-equilibrium effects are absorbed in 'effective' dividend rates, referred to as Non-Equilibrium Dividends (NEDs), to be used in the Black-Scholes formulas entering the mixture. The following Sects. 4.3 and 4.4 present, respectively, a toy calibration to simulated Black-Scholes option prices, and calibration to real data on SPY and SPX options. The final Section 5 concludes. Additional materials are presented in Appendices A to E.

³Langevin dynamics with a cubic potential was previously considered by Bouchaud and Cont [4], however for a different dependent variable (the speed of a market price instead of returns), and applied to modeling of market bubbles and crashes. Related ideas were also discussed by Sornette [31].

⁴The approach of this paper can also be viewed as partially inspired by machine learning paradigms, because it relies on a Gaussian mixture parametrization of a prime modeling objective - which in our case is given by a ground state wave function Ψ_0 . A similar approach to the one developed in this paper can also be applied to other dynamic systems.

2 Langevin dynamics, double well potential, SUSY and the NES

2.1 Langevin dynamics: the Fokker-Planck and Schrödinger pictures

Let S_t be the value of a market index at time t . A period- T log-return y_t is defined as follows

$$y_t = \log \frac{S_t}{S_{t-T}} \quad (1)$$

In this paper, we focus on modeling dynamic distributions of y_t rather than distributions of market value (or a stock price) S_t . The reason is that unlike price dynamics which are non-stationary due to a market or stock drift, returns dynamics can be either stationary or non-stationary. If we define dynamics in terms of log-returns y_t instead of prices S_t , we can differentiate between regimes of stationary vs non-stationary returns, which would be impossible if a model is formulated in terms of prices S_t . As an interplay between these regimes is a key ingredient of analysis in this paper, we explore dynamics of log-returns y_t rather than prices S_t . On the other hand, as $y_T = \log(S_T/S_0)$, knowing a time- T distribution of y_T also gives a distribution of S_T .

We use the Langevin approach to describe continuous-time stochastic dynamics of market returns y_t , where dynamics are determined by an (overdamped) Langevin equation [24]:

$$dy_t = -\frac{\partial V(y_t)}{\partial y_t} dt + h dW_t \quad (2)$$

where h is a volatility parameter, W_t is a standard Brownian motion, and $V(y)$ is an interaction potential. In general, $V(y)$ is a non-linear function whose structure is either deduced from underlying microscopic dynamics, or alternatively postulated based on phenomenological grounds. In particular, a quadratic potential $V(y) = \frac{1}{2}\omega^2(y - y_\star)^2$ gives rise to a linear drift $\mu(y) = -\partial V/\partial y$, producing a familiar Ornstein-Uhlenbeck (OU) process as a special choice for the Langevin dynamics (2). While a different specification of the interaction potential $V(y)$ with higher-order non-linearities will be presented below, for now we will proceed with a general development applicable for an arbitrary potential $V(y)$. The only assumptions used in this section is that a minimum value of the potential is zero, i.e. $V(y_\star) = 0$ where y_\star stands for a minimum point of $V(y)$, and that the potential $V(y)$ rises as $y \rightarrow \pm\infty$ at least as fast as $V(y) \sim y^2$. The last assumption is needed to ensure the existence of a stationary solution to the dynamics.

Transition probabilities $p(y, t|y_0)$ to be at a certain state $y = y_t$ at time t starting with an initial position y_0 at time $t = 0$ satisfy a Fokker-Planck equation (FPE) corresponding to the Langevin equation (2)

$$\frac{\partial p(y, t|y_0)}{\partial t} = \frac{\partial}{\partial y} \left[\frac{\partial V(y)}{\partial y} p(y, t|y_0) \right] + \frac{h^2}{2} \frac{\partial^2}{\partial y^2} p(y, t|y_0) \quad (3)$$

Alongside the transition probability density $p(y, t|y_0)$ that satisfies the FPE (3), it proves useful to consider a related transition density obtained if we used an inverted potential $-V(y)$ in the Langevin equation (2). Denoting such transition density $p_+(y, t|y_0)$ and using the notation $p_-(y, t|y_0)$ for the solution of the original FPE (3), the pair $p_\pm(y, t|y_0)$ satisfies a pair of Fokker-Planck equations that can be compactly written as follows:

$$\frac{\partial p_\pm(y, t|y_0)}{\partial t} = \mp \frac{\partial}{\partial y} \left[\frac{\partial V(y)}{\partial y} p_\pm(y, t|y_0) \right] + \frac{h^2}{2} \frac{\partial^2}{\partial y^2} p_\pm(y, t|y_0) \quad (4)$$

with the initial condition $p_\pm(y, 0|y_0) = \delta(y - y_0)$. We use the following ansatz to solve Eqs.(4) (see e.g. [33]):

$$p_\pm(y, t|y_0) = e^{\pm \frac{V(y) - V(y_0)}{h^2}} \Psi_\pm(y, t|y_0). \quad (5)$$

Using this in Eq.(4) produces two imaginary time Schrödinger equations (SE) for $\Psi_{\pm}(y, t|y_0)$:

$$-h^2 \frac{\partial \Psi_{\pm}(y, t|y_0)}{\partial t} = \mathcal{H}_{\pm} \Psi_{\pm}(y, t|y_0), \quad (6)$$

where h^2 serves as a Planck constant \hbar , and \mathcal{H}_{\pm} are the Hamiltonians

$$\mathcal{H}_{\pm} = -\frac{h^4}{2} \frac{\partial^2}{\partial y^2} + \frac{1}{2} \left(\frac{\partial V}{\partial y} \right)^2 \pm \frac{1}{2} h^2 \frac{\partial^2 V}{\partial y^2} \equiv -\frac{h^4}{2} \frac{\partial^2}{\partial y^2} + U_{\pm}(y). \quad (7)$$

Note that the Hamiltonian \mathcal{H}_- transforms into the partner Hamiltonian \mathcal{H}_+ if we flip the sign of the potential $V(y) \rightarrow -V(y)$. Further properties of the pair of Hamiltonians \mathcal{H}_{\pm} will be explored in the next section, while here we focus on the 'prime' Hamiltonian \mathcal{H}_- corresponding to the initial FPE (3).

Let $\{\Psi_n^-\}$ be a complete set of eigenstates of the Hamiltonian H_- with eigenvalues E_n^- :

$$\mathcal{H}_- \Psi_n^- = E_n^- \Psi_n^-, \quad \sum_n \Psi_n^-(x) \Psi_n^-(y) = \delta(x - y). \quad (8)$$

We assume here a discrete spectrum corresponding to a motion in a bounded domain, so that the set of values $E_n^{(-)}$ is enumerable by integer values $n = 0, 1, \dots$. We can now expand the wave function of the time dependent SE (6) in stationary states (quantum-mechanical wave functions, or WF's) $\{\Psi_n^-\}$:

$$\Psi_{\pm}(y, t|y_0) = \sum_{n=0}^{\infty} c_n^{\pm} e^{-\frac{t E_n^-}{h^2}} \Psi_n^-(y) \quad (9)$$

where coefficients c_n^{\pm} should be found from the initial condition on $\Psi_{\pm}(y, t|y_0)$ which can be read off the initial condition $p_{\pm}(y, 0|y_0) = \delta(y - y_0)$ and Eq.(5):

$$c_n^{\pm} = \int_{-\infty}^{\infty} \Psi_n^-(y) \Psi_{\pm}(y, 0|y_0) = e^{\pm \frac{V(y) - V(y_0)}{h^2}} \quad (10)$$

Combining Eqs.(5), (9) and (10), we obtain the spectral decomposition of the original FPE (see e.g. [33]):

$$p(y, t|y_0) = e^{-\frac{V(y) - V(y_0)}{h^2}} \sum_{n=0}^{\infty} e^{-\frac{t E_n^-}{h^2}} \Psi_n^-(y) \Psi_n^-(y_0). \quad (11)$$

When $t \rightarrow \infty$, only one term with the lowest energy survives in the sum in Eq.(11). As the potential $U_-(y)$ is bounded below by zero, the lowest state, if it exists, would be a state $\Psi_0^-(y)$ with zero energy $E_0^- = 0$. In our setting, we assume that a potential $V(y)$ is such that a normalizable zero energy state $\Psi_0^-(y)$ does exist. Retaining only two leading terms in the expansion (11) and defining $\Delta E := E_1^- - E_0^- = E_1^-$ as an energy splitting between the lowest and the first excited states, we can write it in the following form:

$$p(y, t|y_0) = e^{-\frac{V(y) - V(y_0)}{h^2}} \left[\Psi_0^-(y) \Psi_0^-(y_0) + e^{-\frac{t \Delta E}{h^2}} \Psi_1^-(y) \Psi_1^-(y_0) + \dots \right] \quad (12)$$

The last expression produces both time-dependent and stationary probability densities for the original problem corresponding to the Langevin equation (2) and the FPE (3).⁵ In particular, a stationary distribution is obtained by taking a limit $t \rightarrow \infty$, where only the first term survives.⁶ On the other

⁵If a lowest energy state has a positive energy $E_0^{(-)} > 0$, this would modify Eq.(12) by a time-decay factor $e^{-t E_0^{(-)}/h^2}$, indicating a metastability of an initial state y_0 that would decay with the decay rate $E_0^{(-)}/h^2$.

⁶An apparent remaining dependence on the initial position y_0 in the limit $t \rightarrow \infty$ of Eq.(12) is spurious and will be shown to cancel out in the next section.

hand, for finite values $t < \infty$, Eq.(12) describes a pre-asymptotic behavior en route to a stationary state, where a time-dependent correction is given by the second term in (12). At yet shorter times, higher-order corrections omitted in (12) may become important.

The spectral representation (11) (or its approximation (12)) that gives a decomposition of the solution of the FPE (3) in terms of eigenvalues of the SE (6) is well known in the literature. With a conventional approach, one starts with defining a potential $V(y)$, which is then used to find a Schrödinger Hamiltonian \mathcal{H}_- , and then the latter is used to compute eigenvalues Ψ_n^- . In the next section, we will present an alternative approach that provides a more direct link between the FPE transition density $p(y, t|y_0)$ and wave functions Ψ_n^- . As will be shown next, the quantum-mechanical wave functions Ψ_n^- serve as 'half-probabilities', in the sense that the FP density $p(y, t|y_0)$ is related to squares of Ψ_n^- , in a close analogy to how a square of a wave function in the conventional quantum mechanics is interpreted as a probability density of a quantum mechanical particle.

2.2 Dynamics from statics: SUSY and half-probability distributions

To obtain a different representation of an approximate spectral decomposition (12), we return to the analysis of the pair of Hamiltonians (7). The first observation is that a special form of the potentials $U_{\pm}(y)$ in the Schrödinger Hamiltonians \mathcal{H}_{\pm} enables their factorization into two first-order operators as follows:

$$\mathcal{H}_- = \mathcal{A}^+ \mathcal{A}, \quad \mathcal{H}_+ = \mathcal{A} \mathcal{A}^+ \quad (13)$$

where

$$\mathcal{A} = \frac{h^2}{\sqrt{2}} \frac{\partial}{\partial y} + \mathcal{W}(y), \quad \mathcal{A}^+ = -\frac{h^2}{\sqrt{2}} \frac{\partial}{\partial y} + \mathcal{W}(y), \quad \mathcal{W}(y) := \frac{1}{\sqrt{2}} \frac{\partial V}{\partial y} \quad (14)$$

The factorization properties (13) are well known within supersymmetric quantum mechanics (SUSY QM) of Witten [34]. The reason that the same mathematical construction arises in our problem is that the Schrödinger equation (6) for the FPE possesses hidden supersymmetry (SUSY) [5], that makes it mathematically identical to the Euclidean supersymmetric quantum mechanics (SUSY QM), with h^2 playing the role of the Planck constant \hbar . Using the standard nomenclature in the literature, we will refer to $\mathcal{W}(y) := \frac{1}{\sqrt{2}} \frac{\partial V}{\partial y}$ as a *superpotential*.

The factorization property (13) comes very handy to find a zero-energy eigenstate $\Psi_0(y) = \Psi_0^-(y)$ of \mathcal{H}_- with $E_0^- = 0$, as it enables replacing a second-order ODE $\mathcal{H}_- \Psi_0 = 0$ by a first order equation $\mathcal{A} \Psi_0 = 0$, or more explicitly,

$$\frac{h^2}{\sqrt{2}} \frac{\partial \Psi_0(y)}{\partial y} + \mathcal{W}(y) \Psi_0(y) = 0 \quad (15)$$

The conventional use of this equation is to integrate it to obtain an expression of the zero-energy state $\Psi_0(y)$ in terms of the superpotential $\mathcal{W}(y)$:

$$\Psi_0(y) = C e^{-\frac{\sqrt{2}}{h^2} \int_0^y \mathcal{W}(z) dz} = C e^{-\frac{V(y)}{h^2}} \quad (16)$$

where C is a normalization constant. On the other hand, Eq.(15) can also be used in reverse in order to express the superpotential $\mathcal{W}(y)$ in terms of $\Psi_0^-(y)$:

$$\mathcal{W}(y) = -\frac{h^2}{\sqrt{2}} \frac{d}{dy} \log \Psi_0(y) \quad (17)$$

Therefore, if a zero-energy wave function $\Psi_0(y) = \Psi_0^-(y)$ of \mathcal{H}_- is known, the superpotential $\mathcal{W}(y)$ is fixed in terms of this function. Moreover, as $\mathcal{W}(y) := \frac{1}{\sqrt{2}} \frac{\partial V}{\partial y}$, we also have an expression for the FPE potential $V(y)$ in terms of $\Psi_0(y)$:

$$V(y) = -h^2 \log \Psi_0(y) + V_0 \quad (18)$$

where a constant V_0 is chosen such that the minimum value of $V(y)$ is zero: $V(y_\star) = 0$. As in quantum mechanics a ground state wave function $\Psi_0(y)$ is always strictly positive [23], Eq.(18) is well-defined as long as $\Psi_0(y)$ is a valid ground state function of a quantum mechanical system. The representation (17) is well known in the literature on SUSY QM, see e.g. [10].

In our problem, the utility of the representation (18) can be immediately seen by substituting this expression into Eq.(12). This produces the following relation

$$p(y, t|y_0) = [\Psi_0(y)]^2 + \frac{\Psi_1^-(y_0)}{\Psi_0(y_0)} e^{-\frac{t\Delta E}{\hbar^2}} \Psi_0(y) \Psi_1^-(y) + \dots \quad (19)$$

This relation is also well-known in the literature, see e.g. [33]. It shows that the stationary distribution $p_s(y)$ of y_t as $t \rightarrow \infty$ is given by the square of the ground-state wave function $\Psi_0(y)$: $p_s(y) = [\Psi_0(y)]^2$, in a very similar way to a probabilistic interpretation of quantum mechanics. The stationary density $p_s(y)$ is normalized to one as long as the $\Psi_0(y)$ is squared-normalized. Moreover, due to orthogonality of wave functions $\Psi_0(y)$ and $\Psi_1^-(y)$, the transition density defined by Eq.(19) is automatically normalized to one for arbitrary times t .

Traditionally, Eq.(19) is used from the left to the right, implying that a solution of the FPE equation (3) can be represented as in (19), where the wave functions $\Psi_0(y)$, $\Psi_1^-(y)$ have to be computed by solving the Schrödinger equation with a given Hamiltonian \mathcal{H}_- . In contrast, here we want to use it by reading from the *right* to the *left*, by *defining* the FPE transition density $p(y, t|y_0)$ in terms of a given ground-state wave function $\Psi_0(y)$ viewed as a main modeling primitive, with higher-energy wave functions $\Psi_1^-(y)$ etc. derived from the same $\Psi_0(y)$ as will be explained in details below.

This implies, in particular, that if our only goal is to model a stationary distribution $p_s(y)$ of y_t as $t \rightarrow \infty$, it can be achieved by directly specifying a quantum mechanical ground state wave function $\Psi_0(y)$. A trial ground state wave function $\Psi_0(y)$ can be constructed as a parametric function $\Psi_\theta(y)$, with a functional form and parameters θ chosen such that $\Psi_\theta(y)$ has certain desired properties (such as a shape, symmetries, the local and global behavior at $y \rightarrow \infty$, etc.). Once a parametric function $\Psi_\theta(y)$ is specified, as $p_s(y) = [\Psi_\theta(y)]^2$, defining a stationary distribution thus requires zero extra parameters or calculations.

Note that when viewed on its own, the idea of using the relation $p_s(y) = [\Psi_\theta(y)]^2$ as a way to model a stationary distribution of the FPE dynamics may appear a kind of trivial, as any stationary probability density can be represented as a square of another function. The real value of using the ground state wave function $\Psi_0(y) = \Psi_\theta(y)$ as a prime modeling primitive becomes apparent when it is used jointly with the relation (18) that defines the potential $V(y)$ in terms of $\Psi_0(y)$. Therefore, a parametric specification $\Psi_0(y) = \Psi_\theta(y)$ translates into a parametric choice for $V(y) = V_\theta(y)$ according to Eq.(18). Once the potential $V_\theta(y)$ or the superpotential $\mathcal{W}_\theta(y) = \frac{1}{\sqrt{2}} \frac{\partial V_\theta}{\partial y}$ are defined, the first excited state $\Psi_1^-(y)$ (and higher states) can now be obtained as a solution of the the Schrödinger equation (6). In this equation, the Hamiltonian $\mathcal{H}_- = \mathcal{A}^+ \mathcal{A}$, with \mathcal{A} given by Eq.(14) where the superpotential $\mathcal{W}_\theta(y)$ is defined by Eq.(17). This procedure fixes all time-dependent terms in Eq.(19) in terms of the only model input $\Psi_0(y) = \Psi_\theta(y)$.

This suggests a way of constructing dynamic probability distributions with desirable properties, whose parameters could be interpreted in terms of parameters θ that specify the ground-state wave function $\Psi_\theta(y)$. Note that while defining a superpotential $\mathcal{W}(y)$ in terms of a properly chosen parameterized ground state wave function was previously used to compute tunneling rates with bistable potentials in the context of SUSY QM, see e.g. [10], here we propose a similar idea to model non-linear *stochastic processes* in a tractable way, by specifying them in terms of a parametrized ground state wave function (or a 'half-probability distribution') $\Psi_\theta(y)$. As suggested by Eq.(19), if our only objective is a limiting stationary distribution $p_s(y)$ of y_t as $t \rightarrow \infty$, no further work is needed, and $p_s(y) = [\Psi_\theta(y)]^2$.

To summarize, the representation (19) of a time-dependent transition density of the FPE (3) provides a new tractable way to model non-linear Langevin dynamics (2), where the interaction potential $V(y)$ is defined as in Eq.(18). With this approach, calculation of a stationary density $p_s(y)$ requires no calculation at all, as $p_s(y) = [\Psi_0(y)]^2$. This can be directly computed once a parametrized trial function $\Psi_0(y) = \Psi_\theta(y)$ is specified. To compute a time-dependent pre-asymptotic behavior due to the second term in (19), the only additional step needed is a calculation of the first excited state Ψ_1^- and the energy E_1^- of the Hamiltonian \mathcal{H}_- . In the next section, we will consider a simple model of a ground-state wave function $\Psi_0(y)$ where such calculations become quite tractable.

2.3 NES: A Log-Gaussian Mixture double well potential

To produce an interesting and tractable formulation, we consider a two-component Gaussian mixture as a model of $\Psi_0(y)$, with means μ_1 and $\mu_2 < \mu_1$ and a mixture coefficient $0 \leq a \leq 1$ ⁷ which is additionally scaled by a parameter C chosen such that $\Psi_0(y)$ is squared-integrable with $\int \Psi_0^2(y) dy = 1$:

$$\Psi_0(y) = C [(1-a)\phi(y|\mu_1, \sigma_1^2) + a\phi(y|\mu_2, \sigma_2^2)], \quad \int \Psi_0^2(y) dy = 1 \quad (20)$$

Such a combination of Gaussian densities often provides a good representation of a ground state wave function of a particle in a double well potential. Double well potentials play a special role in statistical physics and quantum mechanics, and are often used to model tunneling phenomena, see e.g. [23] or [36]. In particular, a symmetric double well is described by a symmetric version of (20) with $a = 1/2$ and $\mu_1 = \mu_2$, $\sigma_1 = \sigma_2$. Depending on model parameters, the form (20) can fit a variety of shapes including both a unimodal and bimodal shapes. We are mostly interested in a parameter range when Ψ_0 has a bimodal shape with two maxima separated by a minimum, however it works for either choice. For a later use, it is convenient to represent the WF (20) as a Gaussian pdf multiplied by a factor that asymptotically approaches a constant:

$$\Psi_0(y) = \begin{cases} aC\phi(y|\mu_2, \sigma_2^2)\eta(y) & \text{if } \sigma_2 > \sigma_1 \\ (1-a)C\phi(y|\mu_1, \sigma_1^2)\eta(y) & \text{if } \sigma_2 < \sigma_1 \\ (1-a)C\phi(y|\mu_1, \sigma_1^2)\eta(y) & \text{if } \sigma_2 = \sigma_1, y \geq 0 \\ aC\phi(y|\mu_2, \sigma_2^2)\eta(y) & \text{if } \sigma_2 = \sigma_1, y < 0 \end{cases} \quad (21)$$

where function $\eta(y)$ is defined as follows:

$$\eta(y) = \begin{cases} 1 + \frac{1-a}{a} \exp \{ \log \phi(y|\mu_1, \sigma_1^2) - \log \phi(y|\mu_2, \sigma_2^2) \} & \text{if } \sigma_2 > \sigma_1 \\ 1 + \frac{a}{1-a} \exp \{ \log \phi(y|\mu_2, \sigma_2^2) - \log \phi(y|\mu_1, \sigma_1^2) \} & \text{if } \sigma_2 < \sigma_1 \\ 1 + \frac{a}{1-a} \exp \{ \log \phi(y|\mu_2, \sigma_1^2) - \log \phi(y|\mu_1, \sigma_1^2) \} & \text{if } \sigma_2 = \sigma_1, y \geq 0 \\ 1 + \frac{1-a}{a} \exp \{ \log \phi(y|\mu_1, \sigma_1^2) - \log \phi(y|\mu_2, \sigma_1^2) \} & \text{if } \sigma_2 = \sigma_1, y < 0 \end{cases} \quad (22)$$

Viewing (20) as an *exact*, rather than an approximate ground state wave function, we can plug it into Eq.(18) to find the explicit form of the Langevin potential $V(y)$:

$$V(y) = -h^2 \log [(1-a)\phi(y|\mu_1, \sigma_1^2) + a\phi(y|\mu_2, \sigma_2^2)] - h^2 \log C + V_0 \quad (23)$$

where again V_0 is a constant chosen such that the minimum value of $V(y)$ is zero. Examples of trial ground state WFs Ψ_0 and resulting potentials $V(y)$ are shown in Fig. 1.

⁷To simplify the notation, all parameters here and in all sections until Sect. 4 are defined per period T , or equivalently by assuming that $T = 1$. In Sect. 4, we will re-parameterize the model in terms of annualized model parameters.

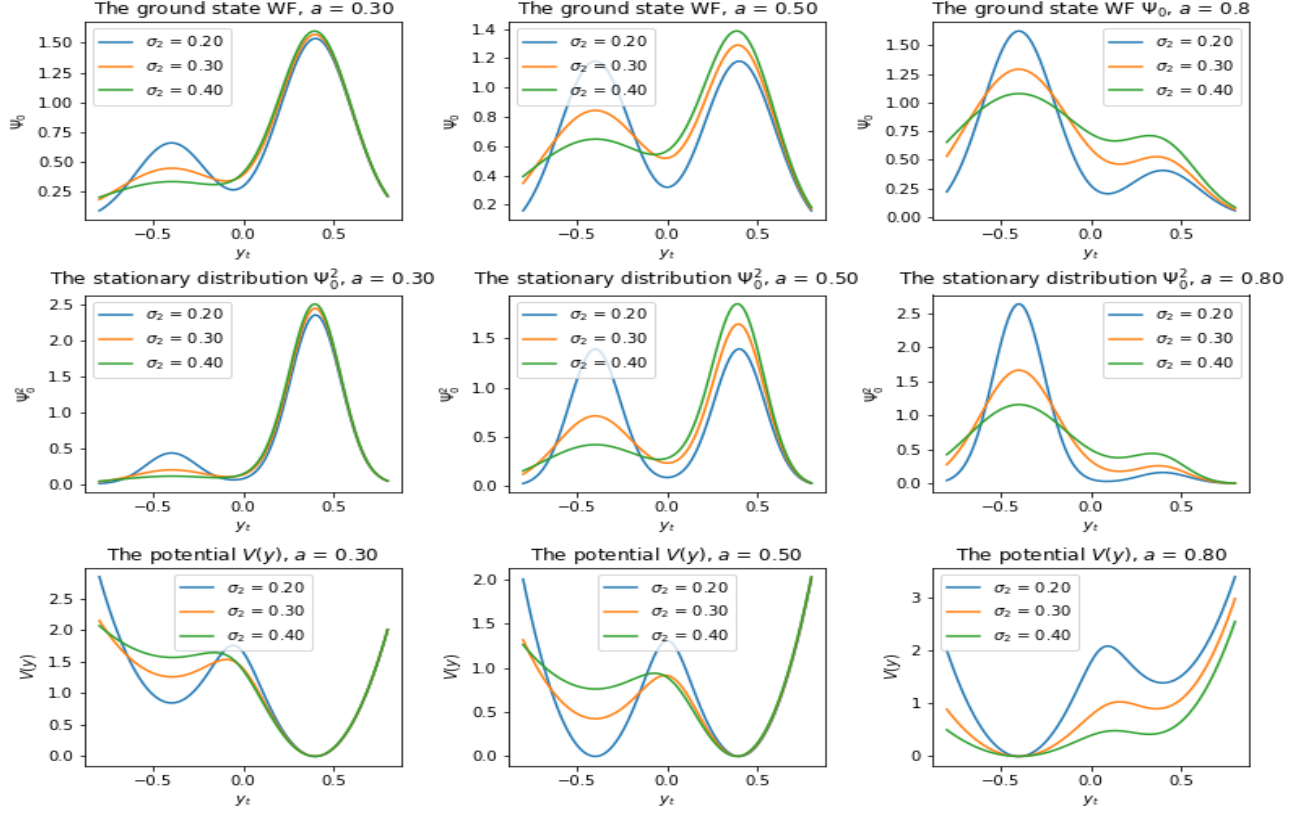


Figure 1: The ground state wave function $\Psi_0(y)$, the stationary distribution $\Psi_0^2(y)$ and the Langevin potential (23) as a function of the market return y_t , for a few values of the asymmetry parameter a , and with different values of parameters σ_2 , with fixed values $\sigma_1 = 0.2, \mu_1 = 0.4, \mu_2 = -0.4$. Graphs on the left describe possible shapes for a 'normal' market regime, where the right minimum is a global minimum. Graphs on the right illustrate a crisis-like regime, when the left minimum becomes a global minimum. Graphs in the middle column describe intermediate scenarios. In particular, when $a = 0.5$ and $\sigma_1 = \sigma_2$, the resulting potential shown in the blue line is symmetric, and can describe a scenario with a spontaneous symmetry breaking.

While this expression produces a non-linear behavior for small positive or negative values of y , its limiting behavior at $y \rightarrow \pm\infty$ is rather simple and coincides with a harmonic (quadratic) potential:

$$V(y)|_{y \rightarrow -\infty} = h^2 \frac{(y - \mu_2)^2}{2\sigma_2^2}, \quad V(y)|_{y \rightarrow \infty} = h^2 \frac{(y - \mu_1)^2}{2\sigma_1^2} \quad (\mu_2 < \mu_1) \quad (24)$$

The fact that the limiting behavior of the potential coincides with a harmonic potential as $y \rightarrow \pm\infty$ means that in this asymptotic regime the model behavior is described by a harmonic oscillator, and thus is fully analytically tractable.

As Gaussian mixtures are known to be universal approximations for an arbitrary non-negative functions given enough components, this implies that an *arbitrary* potential that asymptotically coincides with a harmonic oscillator potential can be represented as a negative logarithm of a Gaussian mixture. We can refer to such class of potentials as Log-Gaussian Mixture (LGM) potentials. In our particular

case, we restrict ourselves to a two-component LGM potential.⁸

Note that while $\Psi_0(y)$ is proportional to a *two*-component Gaussian mixture, its square is proportional to a *three*-component Gaussian mixture:

$$\Psi_0^2(y) = \frac{C^2}{2\sqrt{\pi}} \left[\frac{(1-a)^2}{\sigma_1} \phi\left(y|\mu_1, \frac{\sigma_1^2}{2}\right) + \frac{a^2}{\sigma_2} \phi\left(y|\mu_2, \frac{\sigma_2^2}{2}\right) + 2 \frac{a(1-a)}{\sqrt{\sigma_1^2 + \sigma_2^2}} e^{-\frac{(\mu_1 - \mu_2)^2}{2(\sigma_1^2 + \sigma_2^2)}} \phi\left(y|\mu_3, \frac{\sigma_3^2}{2}\right) \right] \quad (25)$$

where the additional third Gaussian component has the following mean and variance:

$$\mu_3 := \frac{\mu_1 \sigma_2^2 + \mu_2 \sigma_1^2}{\sigma_1^2 + \sigma_2^2}, \quad \frac{\sigma_3^2}{2} = \frac{\sigma_1^2 \sigma_2^2}{\sigma_1^2 + \sigma_2^2} \quad (26)$$

The normalization condition thus fixes the value of the constant C as follows:

$$C^2 = \frac{2\sqrt{\pi}}{\Omega}, \quad \text{where} \quad \Omega = \frac{(1-a)^2}{\sigma_1} + \frac{a^2}{\sigma_2} + 2 \frac{a(1-a)}{\sqrt{\sigma_1^2 + \sigma_2^2}} e^{-\frac{(\mu_1 - \mu_2)^2}{2(\sigma_1^2 + \sigma_2^2)}} \quad (27)$$

Recalling the relation $p_s(y) = [\Psi_0(y)]^2$ and introducing weights

$$\omega_1 := \frac{(1-a)^2}{\sigma_1 \Omega}, \quad \omega_2 := \frac{a^2}{\sigma_2 \Omega}, \quad \omega_3 := \frac{2a(1-a)}{\Omega \sqrt{\sigma_1^2 + \sigma_2^2}} e^{-\frac{(\mu_1 - \mu_2)^2}{2(\sigma_1^2 + \sigma_2^2)}}, \quad \sum_{i=1}^3 \omega_i = 1 \quad (28)$$

we obtain the following three-component Gaussian mixture model for the stationary distribution $p_s(y) = \Psi_0^2(y)$:

$$p_s(y) = \sum_{k=1}^3 \omega_k \phi\left(y|\mu_k, \frac{\sigma_k^2}{2}\right) \quad (29)$$

Note that while a priori defining a three-component Gaussian mixture model requires eight parameters, our approach fixes all parameters of the Gaussian mixture (29) in terms of only five original model parameters $\mu_1, \mu_2, \sigma_1, \sigma_2, a$, or rather four parameters if we set $\mu_1 = \mu_2$ as we will do in most of examples below. Interestingly, the fifth (sixth) model parameter h drops off in the expression for the stationary density $p_s(y)$, and only appears when treating non-stationary effects due to the second term in Eq.(19). In addition, as we will show next, this parameter also controls intensity of transitions between minima of the potential (23). The behavior of moments of the equilibrium distribution is shown in Fig. 2.

2.4 Dynamics with a bistable potential: metastability and instantons

As illustrated in Fig. 1, the NES model may produce a variety of equilibrium distributions including both unimodal and bimodal shapes, where transitions between different shapes are controlled by model parameters. Informally, one can expect that unimodal distributions would be typical for benign markets, while bimodal distributions may arise when a market is distressed or in a crisis. In this section, we focus on a model regime when parameters are such that a ground state $\Psi_0(y)$ is a bimodal function,

⁸A requirement of an asymptotic harmonic oscillator behavior could be seen as a potential limitation for the LGM class of potentials, as many interesting potentials have a different asymptotic behavior. To this point, we can note that an onset of such a quadratic regime can always be pushed further away by a proper rescaling of the coordinate, while for small or moderate values of a new rescaled argument, the dynamics can still be arbitrarily non-linear, and driven by the number of Gaussian components and their parameters.

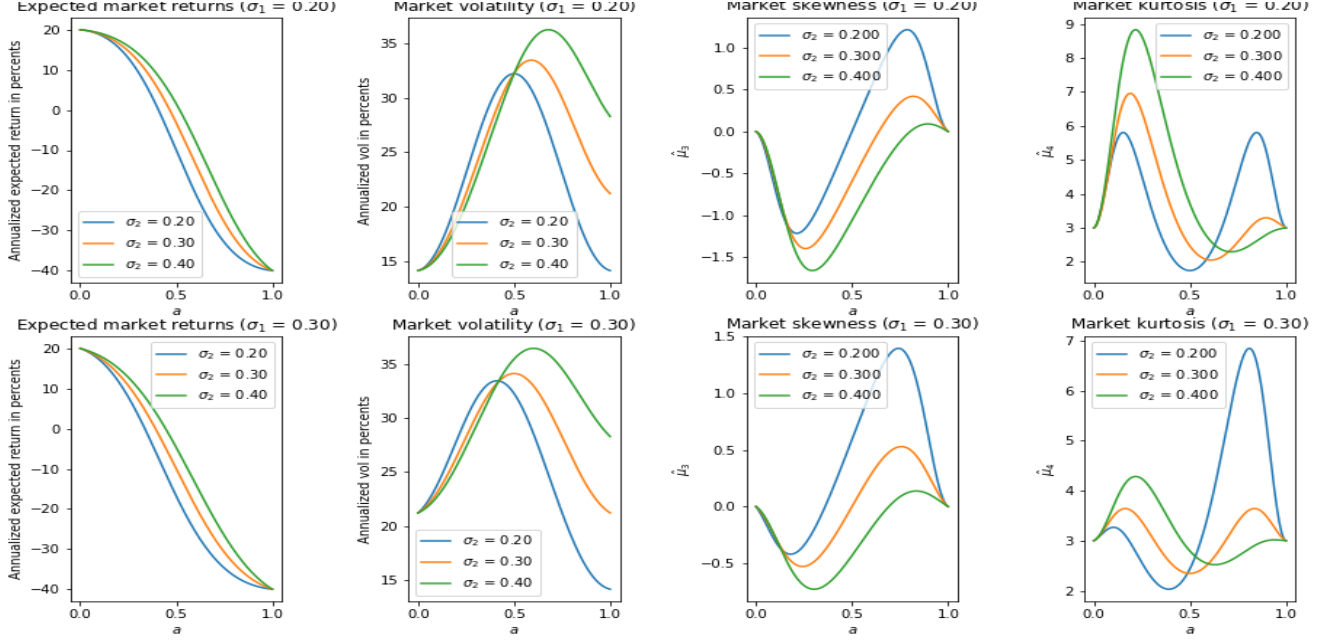


Figure 2: Higher moments of the equilibrium distributions $\Psi_0^2(y)$ as functions of the asymmetry parameter a , and with different values of parameters σ_2 .

corresponding to the market in a crisis or a severe distress. However, the final formulae that we will carry to a final model formulation will be applicable for any choice of Ψ_0 , whether it is unimodal or bimodal, or equivalently for any specification a LGM potential, whether it has a single minimum or two local minima. Formulas that specifically assume a particular choice of the potential will be separately mentioned below.

Assume now that the market is in a regime when $\Psi_0(y)$ has two maxima separated by a local minimum, see Fig. 1. As the logarithmic function is monotonic, Eq.(18) then implies a bimodal Langevin potential $V(y)$, with a local maximum at y_m separating two local minima y_\star and y^\star (the latter coincide with maxima of $\Psi_0(y)$). Here we assume that $y_\star < y_m < y^\star$, and that $V(y_\star) \leq V(y^\star)$, so that y_\star and y^\star are the global and local minima, respectively. The height of a potential barrier faced by a particle initially located at y^\star (i.e. in a local minimum) is $\Delta V := V(y_m) - V(y^\star)$. Such potentials lead to metastability, where a particle initially located near a local minimum y^\star hops over the barrier ΔV as a result of thermal fluctuations. Following physics conventions, we will occasionally refer to states y_\star and y^\star as the true and metastable vacua, respectively. Using this nomenclature, a situation with a potential with a single minimum can be described as a theory with a single stable vacuum.

Using the FPE approach, an escape rate from a metastable minimum of a potential $V(y)$ can be found as the inverse of a mean passage time $\mathcal{T}(y)$ to exit the interval $y = [y_a, y_b]$, viewed as a function of the *backward* (time-zero) variable $y = y_0$. In our case, we can set $y_b = \infty$ and $y_a = y_\star$, with $y_0 > y_\star$, so that $[y_a, y_b] = [y_\star, \infty]$ and $y_\star \leq y_0 \leq \infty$. For a time-homogeneous process, the mean passage time $\mathcal{T}(y)$ satisfies the following backward PDE (see e.g. [11]):

$$-V'(y) \frac{\partial \mathcal{T}(y)}{\partial y} + \frac{h^2}{2} \frac{\partial^2 \mathcal{T}(y)}{\partial y^2} = -1 \quad (30)$$

with boundary conditions $\mathcal{T}(y_\star) = 0$ and $\mathcal{T}'(\infty) = 0$. This equation can be solved by multiplying by an integrating factor $e^{-2V(y)/h^2}$, and then twice integrating the resulting expression using the boundary

conditions. This produces the following well-known relation for the mean passage time $\mathcal{T}(y)$:

$$\mathcal{T}(y_0) = \frac{2}{h^2} \int_{y_\star}^{y_0} dy e^{\frac{2V(y)}{h^2}} \int_y^\infty dz e^{-\frac{2V(z)}{h^2}} \quad (31)$$

This is a general expression valid for any potential $V(y)$ that is sufficiently well-behaved at $y \rightarrow \pm\infty$. In particular, it applies to both cases of a potential with a single minimum or a potential with two local minima separated by a maximum. For the latter case, we obtain a metastable potential $V(y)$ if $V(y_\star) \neq V(y^\star)$, or a potential with spontaneous symmetry breaking if $V(y_\star) = V(y^\star)$.

For a potential with two minima, the mean passage time can be calculated using quadratic expansions of $V(y)$, where the first and second integrals in Eq.(31) are computed using a saddle point approximation with quadratic expansions around, respectively, a maximum y_m and the local minimum y^\star . Such an approximation is justified when $\Delta V/h^2 \gg 1$, i.e. when the barrier is high, while the initial position y_0 is near the local minimum y^\star . This produces the celebrated Kramers escape rate formula for the escape intensity $\lambda = 1/\mathcal{T}$ (see e.g. [11] or [15]):

$$\lambda = \frac{\sqrt{V''(y^\star) |V''(y_m)|}}{2\pi} \exp \left[-\frac{2\Delta V}{h^2} \right] \quad (32)$$

The same result (32) can also be obtained using alternative methods. In particular, with the Schrödinger equation (6), the Kramers escape rate λ can be calculated as $\lambda = \Delta E/h^2$ where $\Delta E = E_1^- - E_0 = E_1^-$ is the energy splitting between a ground state and a first excited state [5]. Within a path integral approach, the energy splitting ΔE can be obtained as a contribution to the path integral due to *instantons* - saddle-point solutions of dynamics obtained in a weak noise (quasi-classical) limit $\hbar \rightarrow 0$ of the Langevin equation (2), where the potential is *inverted*. The instanton equation reads (see Appendix A for more details)

$$\frac{dy_t}{dt} = \frac{\partial V(y_t)}{\partial y_t} \quad (33)$$

While instantons produce the exponential term in (32), the pre-exponential factor is obtained from thermal (or quantum) corrections to an instanton contribution to a transition probability for a bimodal or metastable potential $V(y)$, see e.g. [16]. Note that the Kramers escape rate (32) is non-analytic in the 'Planck constant' h^2 , i.e. it does not have a Taylor expansion around the value $h^2 = 0$. Instantons arising in statistical and quantum mechanics or in quantum field theory produce a similar non-analyticity of transition amplitudes in the Planck constant \hbar or in coupling constants driving non-linearities, see e.g. [7]. This means that instantons are *non-perturbative* solutions that can not be found to any order of a perturbation theory in \hbar . On the other hand, using methods of supersymmetry for analysis of metastability in the Fokker-Planck dynamics with a bistable potential, the same results as obtained from instanton calculus can also be obtained using a pure quantum mechanical approach, as was shown in [5].

With our approach where the ground state wave function is the main modeling primitive, we can express $\mathcal{T}(y)$ in Eq.(31) by substituting there Eq.(18). This gives

$$\mathcal{T}(y_c) = \frac{2}{h^2} \int_{y_\star}^{y_0} \frac{dy}{\Psi_0^2(y)} \int_y^\infty dz \Psi_0^2(z) \quad (34)$$

Note that unlike Eq.(32) which only applies for a bistable potential, the last expression (34) is applicable for either a bistable potential or a potential with a single minimum. In addition, numerical integration in Eq.(34) can be done with arbitrary precision, unlike the Kramers relation (32) which is based on the saddle point approximation and the presence of two minima of the potential. Therefore, we will use Eq.(34) instead of (32) in a practical implementation of the model to be presented below.

Interestingly, the last relation (34) suggests that when Ψ_0^2 is provided as an input that does not depend explicitly on parameter h , then the whole expression depends on h as h^{-2} , which means that the escape rate $\lambda = 1/\mathcal{T}$ is proportional to the 'Planck constant' h^2 . We will return to this remark below.

While Eq.(34) is general and applies for any ground state WF Ψ_0 , it can be approximately calculated analytically for a bistable potential, producing corrections to the Kramers relation (32). To show this, we use the expression for $p_s(y) = [\Psi_0(y)]^2$ given for the trial function (20) by Eq.(29), and compute the inner integral in (34) explicitly:

$$\int_y^\infty dz \Psi_0^2(z) = \sum_{k=1}^3 \omega_k \mathcal{N}\left(\frac{\sqrt{2}(\mu_k - y)}{\sigma_k}\right) \quad (35)$$

where $\mathcal{N}(\cdot)$ stands for the cumulative normal distribution. We approximate the outer integral in (34) by reverting to its previous expression in Eq.(31), and expanding the integrand around its maximum at y_m , while simultaneously replacing the integration limits by infinities. This gives

$$\mathcal{T}(y_0) = \frac{2}{h^2 C^2} e^{\frac{2V(y_m)}{h^2}} \int_{-\infty}^\infty e^{-\frac{(y-y_m)^2}{2\sigma_m^2}} \int_y^\infty dz \Psi_0^2(z) \quad (36)$$

where

$$\sigma_m^2 = \frac{h^2}{2|V''(y_m)|}, \quad \frac{1}{C^2} = \int_{-\infty}^\infty e^{-\frac{2V(y)}{h^2}} dy \simeq \sqrt{\frac{2\pi h^2}{2V''(y^*)}} e^{-\frac{2V(y^*)}{h^2}} \quad (37)$$

Here we replaced the exact expression (27) for the normalization constant C by its Gaussian approximation obtained using a quadratic expansion of $V(y)$ around its local minimum y^* . Using Eq.(35), the integral in Eq.(36) can be computed analytically using the formula⁹

$$\int_{-\infty}^\infty \phi(x) \mathcal{N}(a + bx) dx = \mathcal{N}\left(\frac{a}{\sqrt{1+b^2}}\right) \quad (38)$$

This produces the final analytical approximation for the mean passage time, which applies when an initial position y_0 is near the local minimum y^* :

$$\mathcal{T} = \frac{2\pi}{\sqrt{V''(y^*)|V''(y_m)|}} e^{\frac{2\Delta V}{h^2}} \sum_{k=1}^3 \omega_k \mathcal{N}\left(\frac{\sqrt{2}(\mu_k - y_m)}{\sqrt{\sigma_k^2 + 2\sigma_m^2}}\right) \quad (39)$$

When the arguments of cumulative normal functions in this relation can be approximated by infinities (which is formally obtained in the limit the limit $\mu_k - y_m \rightarrow \infty$ or alternatively $\sigma_k, \sigma_m \rightarrow 0$), this expression produces the same formula (32) for the escape rate $\lambda = 1/\mathcal{T}$. Note that a dependence on the initial position y_0 is neglected in Eq.(39) within the saddle-point approximation. A direct numerical integration in Eq.(34) (which is used for a practical implementation, as was mentioned above) shows that the saddle-point approximation becomes less accurate for smaller initial values y_0 , see Fig. 3.

It is instructive to check how the mean passage time (39) depends on the 'Planck constant' h^2 . Note that σ_m defined in Eq.(37) is actually independent of h as implied by (18). As other parameters entering the sum do not depend on h while $V''(y) \sim h^2$ (see Eq.(23)), we have $\mathcal{T} \sim h^{-2}$. As was mentioned above, the same parametric dependence can also be seen directly from Eq.(34).

Therefore, parameter h^2 controls the escape rate to a stable vacuum starting with a metastable vacuum. On the other hand, note that h^2 does *not* appear in the trial wave function (20) or the stationary distribution

⁹See e.g. https://en.wikipedia.org/wiki/List_of_integrals_of_Gaussian_functions#CITEREFOWen1980.

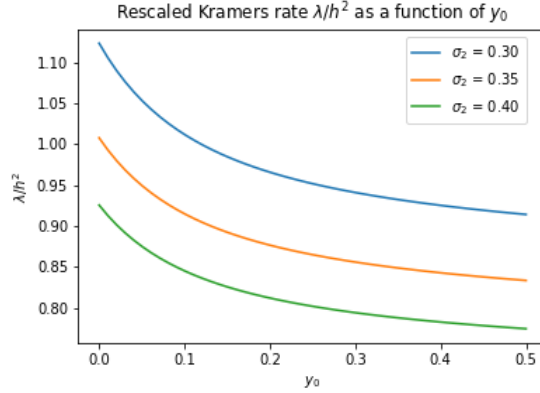


Figure 3: Rescaled Kramers rate $\lambda/h^2 = 1/(\mathcal{T}h^2)$ as a function of the initial position y_0 computed by a numerical integration in Eq.(34). Model parameters used here are $\mu_1 = -\mu_2 = 0.2$, $a = 0.2$, $\sigma_1 = 0.2$.

(29). This does not mean, of course, that properties of a stationary state are not affected by the volatility parameter h , but rather means that with our method of a direct parameterization of the trial wave function (20), its impact on an equilibrium distribution is already incorporated in other model parameters.¹⁰ With this parametrization, the Kramers escape rate λ is equal to h^2 times a *fixed* function of other model parameters, which is illustrated in Fig. 3. As will be shown in the next section, parameter h^2 also appears in pre-asymptotic corrections to the asymptotic (stationary) behavior of the model, and is therefore related to the speed of a relaxation to such an equilibrium state.

3 Computing dynamic corrections with SUSY and the NES

3.1 Supersymmetry and dynamics

So far, our discussion was centered around properties of a stationary distribution (20) that corresponds to an asymptotic (at time $t \rightarrow \infty$) behavior of the FP transition density $p(y, t|y_0)$ in the Langevin model with the potential $V(y)$ given in terms of a ground state WF $\Psi_0(y)$ in Eq.(23). As was discussed above, using a parametric model $\Psi_0(y) = \Psi_\theta(y)$ (where in our case θ stands for all parameters entering Eq.(20)) is very convenient as it provides a direct answer to the problem of finding the asymptotic behavior of the model (assuming all parameters are kept fixed) as $t \rightarrow \infty$. As can be seen from Eq.(19), the equilibrium distribution p_s that describes this limit is given by $\Psi_0^2(y)$, so that no further work is needed to find it.

Therefore, when the stationary distribution $\Psi_0^2(y)$ is an input, rather than an output in a model, the burden of computing the *dynamics* is considerably reduced - all we need to find according to Eq.(19) are higher-energy states $\Psi_n^-(y)$ with $n = 1, 2, \dots$, and their energies E_n^- . They should be computed as solution of the the Schrödinger equation (6). In this equation, the Hamiltonian $\mathcal{H}_- = \mathcal{A}^+ \mathcal{A}$, with \mathcal{A} given by Eq.(14) where the superpotential $\mathcal{W}_\theta(y)$ is defined by Eq.(17).

This procedure fixes all time-dependent terms in Eq.(19) in terms of the only model input $\Psi_0(y) = \Psi_\theta(y)$. The challenging part is to actually compute these higher-energy states WFs $\Psi_n^-(y)$ with $n = 1, 2, \dots$. For some potential, the energy split $\Delta E = E_1^- - E_0$ can be very small, that may give rise to

¹⁰This can be also be simply seen in the original FPE equation (3): if we re-define the potential $V(y) = -h^2 U(y)$ where $U(y)$ is another potential, and then look for a stationary solution, the constant h^2 drops out in the resulting stationary distribution formula when expressed in terms of $U(x)$. It does not imply, of course, that h^2 magically disappears from the problem, but simply means that for a stationary distribution, it can be formally absorbed into parameters defining the new potential $U(y)$.

substantial challenges when computing it, along with computing WFs of excited states using various approximation methods. Furthermore, while many approximate methods of quantum mechanics work well for a ground state of a QM system, they become harder to use (or not usable at all) for higher states.

Supersymmetry (SUSY) is known to offer very efficient computational methods to solve such problem, which were applied to various problems in SUSY QM and classical stochastic systems, see e.g. [8] and [21], respectively. Supersymmetry of the Hamiltonians \mathcal{H}_\pm implies that all eigenstates of \mathcal{H}_- should be degenerate in energy with eigenstates of the SUSY partner Hamiltonian \mathcal{H}_+ , except possibly for a 'vacuum' state with energy $E_0^- = 0$ [34]. Such zero-energy ground state would be unpaired, while all higher states would be doubly degenerate between the SUSY partner Hamiltonians \mathcal{H}_\pm according to the following relations (see e.g. [8] or [21], or Appendix B for a short summary):

$$\begin{aligned}\mathcal{H}_- \Psi_0^- &= \mathcal{A} \Psi_0^- = 0, \quad E_0^- = 0 \\ \Psi_{n+1}^- &= (E_n^+)^{-1/2} \mathcal{A}^+ \Psi_n^+, \quad \Psi_n^+ = (E_{n+1}^-)^{-1/2} \mathcal{A} \Psi_{n+1}^-, \quad n = 0, 1, \dots \\ E_{n+1}^- &= E_n^+, \quad n = 0, 1, \dots\end{aligned}\tag{40}$$

These relations assume that a zero-energy state Ψ_0^- exists. In certain models, Hamiltonians \mathcal{H}_\pm can be supersymmetric, while a ground state Ψ_0^- has a non-zero energy $E_0^- > 0$. Such scenarios correspond to a spontaneous breakdown of SUSY [34]. For such models, supersymmetry is a symmetry of a Hamiltonian but not of a ground state of that Hamiltonian. On the other hand, an unbroken SUSY is characterized by the existence of a normalizable ground state Ψ_0 with strictly zero energy $E_0 = 0$. For SUSY to be unbroken, the derivative of the superpotential $V'(y) = \partial V / \partial y$ should have different signs at $y = \pm\infty$, which means that it should have an odd number of zeros at real values of y [34]. In our problem, SUSY is *not* spontaneously broken by design, as the ground state WF $\Psi_0(y)$ defined in (20) has a zero energy by construction, and the superpotential $\mathcal{W}(y)$ in Eq.(17) does have different signs at $y = \pm\infty$.

Therefore, we can use the SUSY relations to compute Ψ_1^- (and other higher states, if needed) as described above. The reason SUSY is helpful in practice is that it allows one to replace a hard problem of computing a first excited state for the Hamiltonian $\mathcal{H}_- = \mathcal{A}^+ \mathcal{A}$ by a simpler problem of computing a ground state WF for its SUSY partner $\mathcal{H}_+ = \mathcal{A} \mathcal{A}^+$. Once the ground state WF Ψ_0^+ of the Hamiltonian \mathcal{H}_+ is computed using some approximation (e.g. a variational or a perturbation method), the first excited state Ψ_1^- of \mathcal{H}_- can be obtained according to the SUSY relations (40) by applying the SUSY generator \mathcal{A}^+ to Ψ_0^+ , where the superpotential $\mathcal{W}_\theta(y)$ is defined by Eq.(17).

3.2 The ground state of the SUSY partner Hamiltonian \mathcal{H}_+

The first task is therefore to compute (approximately) the ground state WF Ψ_0^+ of the SUSY partner Hamiltonian \mathcal{H}_+ . To this end, note that a candidate ground-state solution of \mathcal{H}_+ is easy to compute from the equation $\mathcal{A}^+ \Psi_0^+ = 0$, whose solution can be obtained by flipping the sign of $V(y)$ in Eq.(16):

$$\Psi_0^+(y) \sim \frac{1}{\Psi_0(y)} \sim \exp \left[\frac{V(y)}{h^2} \right].\tag{41}$$

However, this cannot be a right zero energy solution because it diverges as $y \rightarrow \pm\infty$, and thus is not normalizable. The divergence can be removed if we consider the following ansatz [8, 21]:

$$\Psi_+(y) = \begin{cases} \frac{1}{2I_+} \frac{1}{\Psi_0(y)} \int_y^\infty dz [\Psi_0(z)]^2 & \text{for } y > 0 \\ \frac{1}{2I_-} \frac{1}{\Psi_0(y)} \int_{-\infty}^y dz [\Psi_0(z)]^2 & \text{for } y < 0 \end{cases}\tag{42}$$

where

$$I_+ = \int_0^\infty dz \Psi_0^2(z) \quad I_- = \int_{-\infty}^0 dz \Psi_0^2(z)\tag{43}$$

The ansatz (42) can now be computed in closed form using the ground state WF (20). Using Eq.(29), we obtain

$$\Psi_+(y) = \begin{cases} \frac{1}{2I_+} \frac{1}{\Psi_0(y)} \sum_{k=1}^3 \omega_k \mathcal{N}\left(\frac{\sqrt{2}(\mu_k - y)}{\sigma_k}\right), & \text{for } y > 0 \\ \frac{1}{2I_-} \frac{1}{\Psi_0(y)} \sum_{k=1}^3 \omega_k \mathcal{N}\left(\frac{\sqrt{2}(y - \mu_k)}{\sigma_k}\right), & \text{for } y < 0 \end{cases} \quad (44)$$

with

$$I_+ = \sum_{k=1}^3 \omega_k \mathcal{N}\left(\frac{\sqrt{2}\mu_k}{\sigma_k}\right), \quad I_- = \sum_{k=1}^3 \omega_k \mathcal{N}\left(-\frac{\sqrt{2}\mu_k}{\sigma_k}\right) \quad (45)$$

These relations imply that $\Psi_+(0) = \frac{1}{2\Psi_0(0)}$. Note as it stands, Eq.(44) is not very convenient for numerical implementation, as it can produce numerical overflows. A more convenient representation is obtained by using the representation of Ψ_0 given in Eq.(21), and expressing (44) in terms of the complimentary error function $\text{erfc}(x) = 2\mathcal{N}(-\sqrt{2}x)$ and the scaled complementary error function $\text{erfcx}(x) = e^{x^2} \text{erfc}(x)$:

$$\Psi_+(y) = \begin{cases} \frac{\sqrt{2\pi}\sigma_+^2}{4I_+C_+} \sum_{k=1}^3 \omega_k e^{\frac{(y-\mu_+)^2}{2\sigma_+^2} - \frac{(y-\mu_k)^2}{\sigma_k^2} - \log \eta(y)} \text{erfcx}\left(\frac{y-\mu_k}{\sigma_k}\right), & \text{for } y > 0 \\ \frac{\sqrt{2\pi}\sigma_-^2}{4I_-C_-} \sum_{k=1}^3 \omega_k e^{\frac{(y-\mu_-)^2}{2\sigma_-^2} - \frac{(y-\mu_k)^2}{\sigma_k^2} - \log \eta(y)} \text{erfcx}\left(\frac{\mu_k - y}{\sigma_k}\right), & \text{for } y < 0 \end{cases} \quad (46)$$

where

$$\begin{aligned} C_+ &= C_- = aC, \mu_+ = \mu_- = \mu_2, \sigma_+ = \sigma_- = \sigma_2 \text{ if } \sigma_2 > \sigma_1 \\ C_+ &= C_- = (1-a)C, \mu_+ = \mu_- = \mu_1, \sigma_+ = \sigma_- = \sigma_1 \text{ if } \sigma_2 < \sigma_1 \\ C_+ &= (1-a)C, C_- = aC, \mu_+ = \mu_1, \mu_- = \mu_2, \sigma_+ = \sigma_1, \sigma_- = \sigma_2, \text{ if } \sigma_2 = \sigma_1, \end{aligned}$$

As for $x \rightarrow \infty$ $\text{erfcx}(x) \rightarrow (1/\sqrt{\pi})1/x$ while $\eta(y) \rightarrow 1$, this produces the following asymptotic behavior at $y \rightarrow \pm\infty$ (assuming that $\sigma_2 > \sigma_1$):

$$\Psi_+(y) = \begin{cases} \frac{a}{4\pi^{1/4}I_+\sqrt{\Omega}} \frac{1}{y-\mu_2} e^{-(y-\mu_2)^2/(2\sigma_2^2)}, & \text{for } y \rightarrow \infty \\ \frac{1-a}{4\pi^{1/4}I_-\sqrt{\Omega}} \frac{1}{\mu_2-y} e^{-(y-\mu_2)^2/(2\sigma_2^2)}, & \text{for } y \rightarrow -\infty \end{cases} \quad (47)$$

For numerical integration of $\Psi_+(y)$ that would be needed below, multiple calls for function $\text{erfcx}(x)$ can be time-consuming. As an alternative, one can rely on approximate expressions for $\text{erfcx}(x)$, see e.g. [28]. Other ways to simplify calculations will be discussed below.

Note that Eqs.(47) imply that Ψ_+ is square-integrable, as it decays as a Gaussian multiplied by $1/y$. The last relation is actually independent of a particular choice of the potential $V(y)$, as the same functional form of a Gaussian times $1/y$ can also be found if the integrals in (42) are evaluated using a saddle-point approximation around a minimum of a general potential $V(y)$. Assuming that a potential $V(y)$ has a local minimum at point y_\star with a value V_\star and a second derivative V_\star'' at this point, a saddle-point calculation of integrals entering Eq.(42) produces the following result for $y > 0$ (here $u = \sqrt{V_\star''}(y - y_\star)/h$):

$$\Psi_+(y) = \frac{1}{Z} e^{\frac{1}{2}u^2} \mathcal{N}(-\sqrt{2}u) = \frac{1}{2Z} e^{-\frac{1}{2}u^2} \text{erfcx}(u) \xrightarrow{y \rightarrow \infty} \frac{1}{Z} \frac{1}{y - y_\star} e^{-\frac{1}{2} \frac{(y-y_\star)^2}{h^2/V_\star''}} \quad (48)$$

where Z is a normalization constant whose specific expression will not be needed below, and $\text{erfcx}(x) = e^{x^2} \text{erfc}(x)$ is the scaled complementary error function. For negative values $y < 0$, one obtains the same expression with a flipped sign of the argument of $\mathcal{N}(x)$, $\text{erfc}(x)$, $\text{erfcx}(x)$, with y_\star substituted by a local minimum for the region $y < 0$. Assuming that local minima of $V(y)$ are well-separated for the ground state WF (20), their positions are well approximated by values μ_1 and μ_2 for $x < 0$ and $x > 0$, respectively, with $V(\mu_1)'' = h^2/\sigma_1^2$ and $V(\mu_2)'' = h^2/\sigma_2^2$, respectively.

Most of the calculation in this section do not however use the explicit form (44) and proceed with a general definition in Eq.(42), while only relying on the asymptotic behavior (47).

One can easily check that $\Psi_+(y)$ defined in Eq.(42) is continuous at $y = 0$ with $\Psi_+(0) = \frac{1}{2\Psi_0(0)}$, and that $\mathcal{H}_+\Psi_+ = 0$ for $y \neq 0$. For example, by taking $y > 0$, we obtain

$$\begin{aligned}\mathcal{H}_+\Psi_+(y) &= \mathcal{A} \left[-\frac{h^2}{\sqrt{2}} \frac{d\Psi_+(y)}{dy} + \mathcal{W}\Psi_+(y) \right] = \mathcal{A} \left[-\mathcal{W}\Psi_+(y) + \frac{h^2}{\sqrt{2}} \frac{1}{2I_+} \Psi_0(y) + \mathcal{W}\Psi_+(y) \right] \\ &= \frac{h^2}{\sqrt{2}} \frac{1}{2I_+} \mathcal{A}\Psi_0(y) = 0\end{aligned}\quad (49)$$

However, its derivative has a discontinuity at $y = 0$:

$$\lim_{\varepsilon \rightarrow 0} \left. \frac{d\Psi_+(y)}{dy} \right|_{\varepsilon} - \left. \frac{d\Psi_+(y)}{dy} \right|_{-\varepsilon} = \lim_{\varepsilon \rightarrow 0} 2\varepsilon \left. \frac{d^2\Psi_+(y)}{dy^2} \right|_{y=0} = -\frac{\Psi_0(0)}{2} \left[\frac{1}{I_+} + \frac{1}{I_-} \right] = -\frac{\Psi_0(0)}{2I_+I_-} \quad (50)$$

Therefore, Ψ_+ defined in Eq.(42) is not an eigenstate of \mathcal{H}_+ . Instead, Ψ_+ is a zero-energy ground state WF of a singular Hamiltonian \mathcal{H}_s given by

$$\mathcal{H}_s = \mathcal{H}_+ - \frac{2h^4}{I_+I_-} \Psi_0^2(0) \delta(y) \equiv \mathcal{H}_+ - \delta\mathcal{H}, \quad (51)$$

that differs from \mathcal{H}_+ by the δ -function term $\delta\mathcal{H}$. Indeed, with this Hamiltonian we obtain

$$\int dy \Psi_+(y) \mathcal{H}_s \Psi_+(y) = 0, \quad (52)$$

as a result of the fact that $\mathcal{H}_s\Psi_+(y) = \mathcal{H}_+\Psi_+ = 0$ for $y \neq 0$, while finite contributions coming from the discontinuity of the first derivative (50) and the additional δ -function term cancel each other:

$$-\frac{h^4}{2} \int_{-\varepsilon}^{\varepsilon} \Psi_+(y) \frac{d^2\Psi_+(y)}{dy^2} dy - \int_{-\varepsilon}^{\varepsilon} [\Psi_+(y)]^2 \delta\mathcal{H} dy = \frac{h^4}{8} \frac{1}{I_+I_-} - \frac{h^4}{8} \frac{1}{I_+I_-} = 0 \quad (53)$$

Equivalently, we can express \mathcal{H}_+ in terms of \mathcal{H}_s :

$$\mathcal{H}_+ = \mathcal{H}_s + \delta\mathcal{H}, \quad \delta\mathcal{H} := \alpha\delta(y), \quad \alpha := \frac{2h^4}{I_+I_-} \Psi_0^2(0) \quad (54)$$

3.3 Logarithmic Perturbation Theory for the log-wave function

Given the structure of the Hamiltonian \mathcal{H}_+ in Eq.(54), its ground-state eigenvalue and the eigenfunction can be found using quantum mechanical perturbation theory (see e.g. [23]). To this end, we treat the additional term $\delta\mathcal{H}$ as a perturbation around the exactly solvable singular Hamiltonian \mathcal{H}_s . Following the literature on SUSY QM (see e.g. [20, 10]), we use the Logarithmic Perturbation Theory (LPT), instead of a more conventional Rayleigh-Schrödinger (RS) perturbation theory. For a one-dimensional Schrödinger equation, the LPT yields quadrature formulas for energies and wave functions to any given order in the perturbation theory, in a hierarchical scheme. The LPT becomes especially simple for a ground state which is nodeless, and thus can be represented in the form $\psi(x) = \exp[-G(x)/\hbar]$ where $G(x)$ is some continuous function. By inversion of this formula, we have $G(x) = -\hbar \log \psi(x)$, therefore function $G(x)$ can be referred to as a log-wave function (log-WF). The perturbation scheme is then constructed for $g(x) = G'(x) = -\hbar\psi'(x)/\psi(x)$. While the LPT can be shown to be equivalent to the RS perturbation theory [1], it is far more convenient in practice due to its recursive quadrature form and the absence of a

need to compute matrix elements of a perturbation potential. Details of the LPT method are provided in Appendix C.

To the first order in perturbation $\delta\mathcal{H}$, the ground-state energy $E_0^+ = E_1^-$ is given by Eq.(C.7) where we have to substitute $\hbar \rightarrow h^2$, $\alpha \rightarrow 2h^4\Psi_0^2(0)/(I_+I_-)$, and $V_1(y) = \delta(y)$. This gives the same result as the conventional RS perturbation theory (see e.g. [23]):

$$E_0^+ = E_1^- = \alpha \bar{E}_1, \quad \alpha = \frac{2h^4\Psi_0^2(0)}{I_+I_-} \quad (55)$$

$$\bar{E}_1 = \frac{\int_{-\infty}^{\infty} \Psi_+^2(y)\delta(y)dy}{\int_{-\infty}^{\infty} \Psi_+^2(y)dy} = \frac{\Psi_+^2(0)}{\int_{-\infty}^{\infty} \Psi_+^2(y)dy} \simeq \frac{\Psi_+^2(0)}{\int_{-\infty}^{\infty} e^{-\frac{2V}{h^2}} dy \int_{-\infty}^{\infty} e^{\frac{2V}{h^2}} dy}$$

Here the last approximate equality is obtained by assuming that the barrier is high, and therefore the ground state wave function Ψ_0 is concentrated around the minimum of $V(y)$ where the exact form of $V(y)$ is replaced by its approximation around this minimum. In other words, tunneling is neglected when we compute the energy splitting formula (55), similarly to how tunneling is computed in quantum mechanics ([23], Sect. 50). With such assumption, $\Psi_+(y)$ can be approximated as follows: $\Psi_+(y) \simeq 1/\Psi_0^-(y) = 1/C \exp\left[\frac{V(y)}{h^2}\right]$, where $V(y)$ can be approximated by its quadratic expansion around it maximum. The first integral in the denominator in the last expression in (55) comes due to the square of the normalization factor C . As the inverse of expression given in (55) is proportional to \mathcal{T} defined in Eq.(31), such a Gaussian approximation produces the same relation (32) for the escape rate $\lambda = E_1^-/h^2$. Therefore, the classical Kramers escape rate relation can also be obtained using methods of SUSY [5, 21].

For the ground-state wave function $\Psi_0^+(y)$ of the Hamiltonian \mathcal{H}_+ , the LPT produces a perturbative expansion of a 'log-WF' $G(y) = -h^2 \log \Psi_0^+(y)$ in powers of perturbation parameter $\alpha = 2h^4\Psi_0^2(0)/(I_+I_-)$. To the first order in α , the WF $\Psi_0^+(y)$ has the following form:

$$\Psi_0^+(y) = C_1 e^{-\frac{G_0(y)}{h^2} - \frac{\alpha G_1(y)}{h^2}} = C_1 \Psi_+(y) e^{-\frac{\alpha G_1(y)}{h^2}}, \quad \alpha = \frac{2h^4}{I_+I_-} \Psi_0^2(0), \quad (56)$$

where C_1 is a normalization factor to be determined later, $\Psi_+(y)$ is the unperturbed WF defined in (42), and $G_0(y) = -h^2 \log \Psi_+(y)/C_1$ stands for the log-WF of the unperturbed Hamiltonian \mathcal{H}_s .

While a specific expression for the first-order correction $G_1(y)$ will be given momentarily, one should note that within perturbation theory, a first-order approximation of the form (56) is only justified when a first correction $\alpha G_1(x)$ is smaller than an unperturbed log-WF $G_0(x)$:

$$\alpha |G_1(x)| < |G_0(x)|, \quad G_0(x) = -h^2 \log \frac{\Psi_+(x)}{C_1} \quad (57)$$

As implied by Eq.(47), function $G_0(x)$ grows quadratically in the asymptotics: $G_0(x) \propto x^2$ when $x \rightarrow \pm\infty$. On the other hand, as the perturbation potential in our problem is given by a Dirac delta-function centered at $x = 0$, the function $G_1(x)$ that incorporates its effect is expected to decay as $x \rightarrow \pm\infty$. Therefore, using perturbation theory is justified in our problem.

The first-order correction log-WF $G_1(x)$ is determined by the following relations, see Eqs.(C.2) and (C.9):

$$G_1(x) = \begin{cases} \frac{2}{h^2} \int_{-\infty}^x \frac{dy}{\Psi_+^2(y)} \int_{-\infty}^y dz (\bar{E}_1 - \delta(z)) \Psi_+^2(z), & x > 0 \\ -\frac{2}{h^2} \int_{-\infty}^x \frac{dy}{\Psi_+^2(y)} \int_y^{\infty} dz (\bar{E}_1 - \delta(z)) \Psi_+^2(z), & x < 0 \end{cases} \quad (58)$$

We omit here an additive constant that can re-absorbed into the normalization constant C_1 in (56). Using the constraint (55), Eq.(58) can be written in a different form:

$$G_1(x) = \begin{cases} \frac{2\bar{E}_1}{h^2} \left[\int_{-\infty}^0 \frac{dy}{\Psi_+^2(y)} \int_{-\infty}^y dz \Psi_+^2(z) - \int_0^x \frac{dy}{\Psi_+^2(y)} \int_y^{\infty} dz \Psi_+^2(z) \right], & \text{for } x > 0 \\ \frac{2\bar{E}_1}{h^2} \int_{-\infty}^x \frac{dy}{\Psi_+^2(y)} \int_{-\infty}^y dz \Psi_+^2(z), & \text{for } x < 0 \end{cases} \quad (59)$$

Due to Eq.(55), $G_1(x)$ is continuous at $x = 0$ in Eq.(58), as can also be seen in Eq.(59). For the derivative $g_1(x) = G'_1(x)$, we find

$$G'_1(x) = \begin{cases} -\frac{2\bar{E}_1}{h^2} \frac{1}{\Psi_+^2(x)} \int_x^\infty dz \Psi_+^2(z), & \text{for } x > 0 \\ \frac{2\bar{E}_1}{h^2} \frac{1}{\Psi_+^2(x)} \int_{-\infty}^x dz \Psi_+^2(z), & \text{for } x < 0 \end{cases} \quad (60)$$

The derivative $G'_1(x)$ is positive for $x < 0$ and negative for $x > 0$, see Fig. 4. Therefore $G_1(x)$ has a maximum at $x = 0$ with the value

$$G_1(0) = \frac{2\bar{E}_1}{h^2} \int_{-\infty}^0 \frac{dy}{\Psi_+^2(y)} \int_{-\infty}^y dz \Psi_+^2(z) > 0 \quad (61)$$

Note that while $G_1(x)$ is continuous at $x = 0$, its second derivative has a jump: for a small value $\varepsilon \rightarrow 0$, we obtain

$$G''_1(\varepsilon) - G''_1(-\varepsilon) = \frac{2\bar{E}_1}{h^2} + \frac{2\bar{E}_1}{h^2} = \frac{4\bar{E}_1}{h^2}, \quad \varepsilon \rightarrow 0 \quad (62)$$

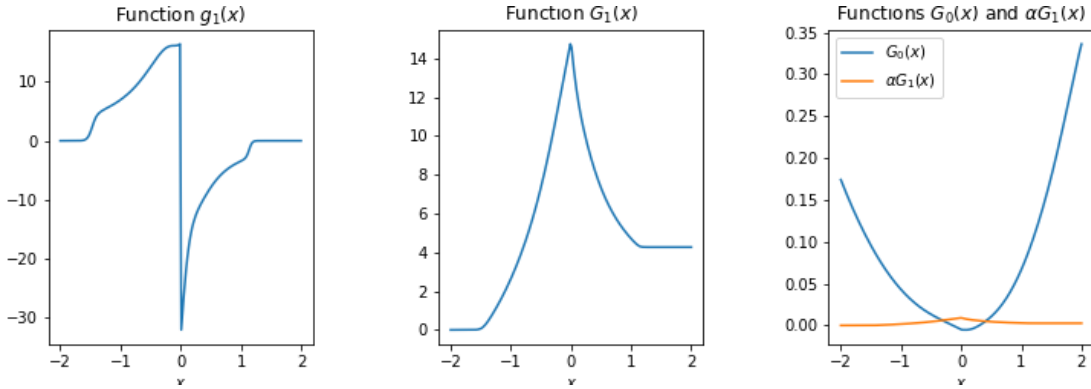


Figure 4: Functions $g_1(x) = G'_1(x)$ (the left graph) and $G_1(x)$ (the graph in the center) obtained by numerical integration of $\Psi_+(y)$ according to Eqs.(60) and (59). The following parameters are used $a = 0.3$, $\mu_1 = 0.4$, $\mu_2 = -0.4$, $\sigma_1 = 0.2$, $\sigma_2 = 0.3$, $h = 0.05$. The graph on the right shows the scaled function $\alpha G_1(x)$ vs the log-WF $G_0(x) = -h^2 \log \Psi_+(x)$ of the unperturbed Hamiltonian \mathcal{H}_s , see Eq.(56). While $G_1(x)$ decays as $x \rightarrow \pm\infty$, $G_0(x)$ grows as a quadratic function.

3.4 The first excited state of \mathcal{H}_-

When the ground state WF of the SUSY partner Hamiltonian \mathcal{H}_+ is computed to the first order of LPT in Eq.(56), we can now use SUSY relations (40) to obtain excited states of \mathcal{H}_- . For the first excited state Ψ_1^- of \mathcal{H}_- , we have the following relation in terms of the ground state Ψ_0^+ of \mathcal{H}_+ :

$$\Psi_1^- = (E_0^+)^{-1/2} \mathcal{A}^+ \Psi_0^+ = (E_0^+)^{-1/2} \left[-\frac{h^2}{\sqrt{2}} \frac{d\Psi_0^+(y)}{dy} + \mathcal{W} \Psi_0^+(y) \right] \quad (63)$$

Substituting here Eqs.(40) and.(56), we obtain

$$\Psi_1^-(y) = \begin{cases} \frac{(E_0^+)^{-1/2}}{\sqrt{2}} \frac{C_1 h^2}{2I_+} \left[\Psi_0(y) e^{-\frac{\alpha G_1(y)}{h^2}} - \frac{1}{\Psi_0(y)} \frac{d}{dy} \left(e^{-\frac{\alpha G_1(y)}{h^2}} \right) \int_y^\infty dz \Psi_0^2(z) \right], & y > 0 \\ \frac{(E_0^+)^{-1/2}}{\sqrt{2}} \frac{C_1 h^2}{2I_-} \left[-\Psi_0(y) e^{-\frac{\alpha G_1(y)}{h^2}} - \frac{1}{\Psi_0(y)} \frac{d}{dy} \left(e^{-\frac{\alpha G_1(y)}{h^2}} \right) \int_{-\infty}^y dz \Psi_0^2(z) \right], & y < 0 \end{cases} \quad (64)$$

We can check that this WF is orthogonal to the ground state WF $\Psi_0 = \Psi_0^-$:

$$\int_{-\infty}^0 dy \Psi_0^-(y) \Psi_1^-(y) + \int_0^{\infty} dy \Psi_0^-(y) \Psi_1^-(y) = -\frac{C_1 h^2}{2\sqrt{2}} e^{-\frac{\alpha G_1(0)}{h^2}} + \frac{C_1 h^2}{2\sqrt{2}} e^{-\frac{\alpha G_1(0)}{h^2}} = 0 \quad (65)$$

One can also check that the first state Ψ_1^- is squared-normalized provided Ψ_0^+ is square-normalized, while the coefficient $(E_0^+)^{-1/2}$ takes care of a proper normalization of Ψ_1^- .

Shapes of Ψ_1^- obtained in our model are illustrated in Fig. 5, along with a ground state WF $\Psi_0 = \Psi_0^-$, and an unperturbed ground state WF Ψ_+ of the partner SUSY Hamiltonian \mathcal{H}_+ . As could be expected, the WF Ψ_1^- of the first excited state resembles the well known WF $\Psi_1 \propto x e^{-m\omega x^2/2\hbar}$ of the first excited state of the quantum mechanical harmonic oscillator [23].

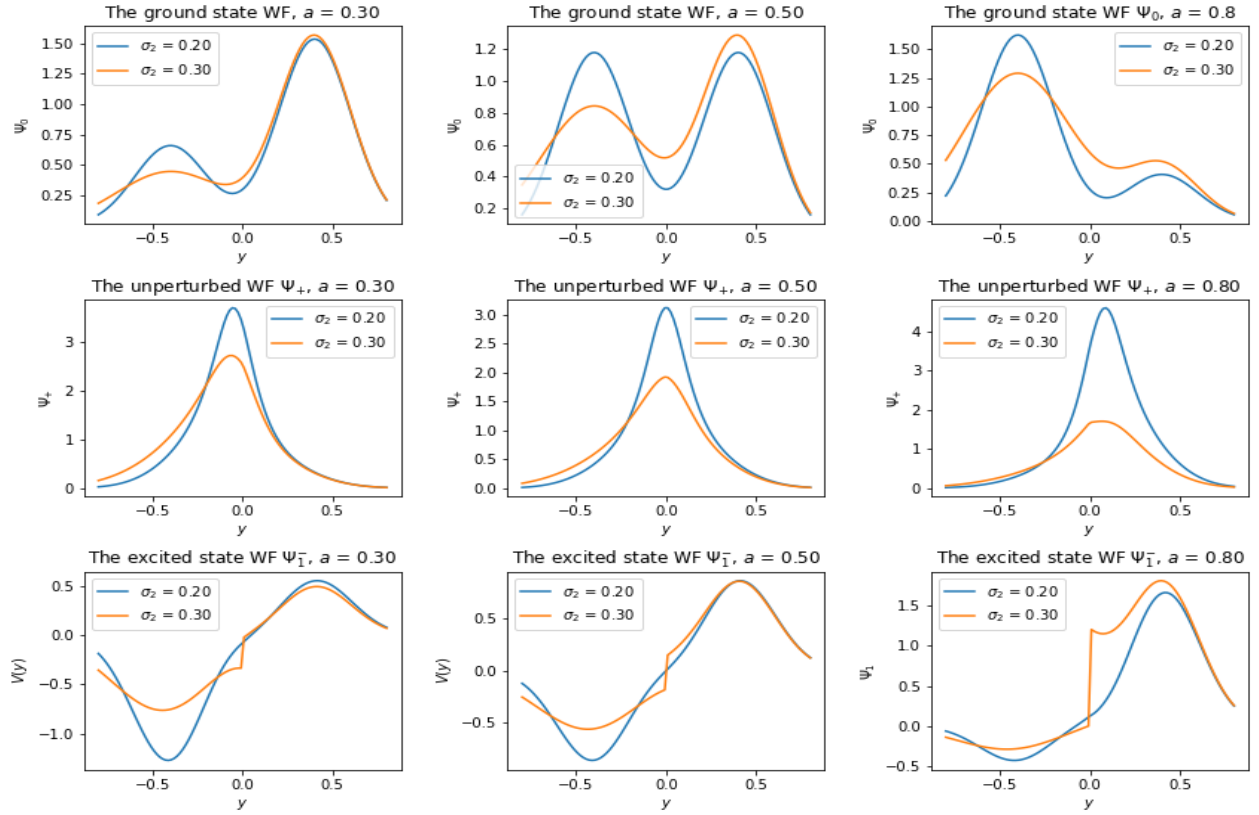


Figure 5: The ground state WF Ψ_0 of the Hamiltonian \mathcal{H}_- , the unperturbed ground state Ψ_+ of the SUSY partner Hamiltonian \mathcal{H}_+ , and the first excited state WF Ψ_1^- of \mathcal{H}_- .

Once the first state Ψ_1^- is computed using SUSY, we are done in terms of computing the leading pre-asymptotic correction to a stationary distribution. It is given by Eq.(19) which we repeat here for convenience:

$$p(y, t|y_0) = \Psi_0^2(y) + \frac{\Psi_1^-(y_0)}{\Psi_0(y_0)} e^{-\frac{t\Delta E}{h^2}} \Psi_0(y) \Psi_1^-(y) + \dots \quad (66)$$

This means that the time-dependent component of the return distribution is given, at a leading pre-asymptotic order, by the product $\Psi_1^-(y) \Psi_1^-(y_0)$. This immediately translates into time-dependent corrections to the variance and skewness of the return distribution.

4 Applications

4.1 NES: Practical implementation

Formulas presented above provide an accurate theoretical scheme of computing the first excited state WF Ψ_1^- in Eq.(64), and hence give an explicit solution for a time-dependent component in the non-stationary return distribution (66). In practice, computing this WF involves a numerical computation of a double integral that defines function $G_1(x)$, see Eq.(58), which may be time-consuming for model calibration when such computations should be done many times. One way to handle such potential challenges that was mentioned above was to use fast numerical approximations to evaluate the scaled complimentary error function $\text{erfcx}(x)$, however this still requires a double numerical integration.

An alternative that might be preferred in practice would be to directly approximate the WF Ψ_1^- . As was mentioned above, it resembles, not accidentally, the first excited state WF $\Psi_1 \propto x e^{-m\omega x^2/2\hbar}$ of a quantum mechanical harmonic oscillator. This suggests that a simple approximation Ψ_1^- would be given by the following expression:

$$\Psi_1^-(y) \simeq \frac{1}{\sigma_M} (y - \bar{y}_M) \Psi_0(y) \quad (67)$$

where \bar{y}_M and σ_M are the mean and standard deviation of the Gaussian mixture defined by Ψ_0^2 :

$$\bar{y}_M = \int dy y \Psi_0^2(y) = \sum_{k=1}^3 \mu_k \omega_k, \quad \sigma_M^2 = \int dy (y - \bar{y})^2 \Psi_0^2(y) = \sum_{k=1}^3 \omega_k (\mu_k^2 + \sigma_k^2) - \bar{y}^2 \quad (68)$$

Substituting (67) into Eq.(66) produces the following simplified form that can be used for practical applications of the model:

$$p(y, t|y_0) = \Psi_0^2(y) [1 + b_t(y - \bar{y}_M)], \quad b_t := \frac{y_0}{\sigma_M} e^{-\lambda t} \quad (69)$$

where we used the definition $\lambda = \frac{\Delta E}{\hbar^2}$ of the Kramers escape rate, where the energy splitting ΔE is computed according to Eq.(55). Note that the density defined by this relation can formally become negative for large negative values of $y - \bar{y}_M$. However, this is an artifact of a reliance on the first-order perturbation theory that was used to derive Eq.(69). As long as perturbation theory is applicable, we have $b_t(y - \bar{y}_M) \ll 1$, and can thus replace $1 + b_t(y - \bar{y}_M) \rightarrow e^{b_t(y - \bar{y}_M)}$ under the same assumptions. Therefore, we can replace (69) by even a simpler form

$$p(y, t|y_0) = C e^{b_t y} \Psi_0^2(y) \quad (70)$$

where the factor $e^{-b_t \bar{y}_M}$ is absorbed into a normalization constant C . When perturbation theory applies, differences between Eqs.(70) and (69) would be negligible as long as all integrals defining observable quantities using the definition (70) are dominated by a region of small y where $b_t |y - \bar{y}_M| \leq 1$. In this case, using (70) instead of (69) would simplify calculations, while any differences could be re-absorbed in slight modifications of model parameters relative to their values in the original equation (69).

While Eq.(70) will be used below for option pricing, it is more illuminating to use the original form (69) to approximate time-dependent contributions to moments of the return distribution. For the mean, variance and skewness of the time-dependent distribution (69), we obtain

$$\begin{aligned} \mathbb{E}[y_t] &= \bar{y} + b_t \sigma_M^2, \quad \sigma_M^2 = \int dy (y - \bar{y})^2 \Psi_0^2(y) \\ \mathbb{E}[(y_t - \bar{y})^2] &= \sigma_M^2 + b_t \mathcal{M}_3, \quad \mathcal{M}_3 = \int dy (y - \bar{y})^3 \Psi_0^2(y) \\ \mathbb{E}[(y_t - \bar{y})^3] &= \mathcal{M}_3 + b_t \mathcal{M}_4, \quad \mathcal{M}_4 = \int dy (y - \bar{y})^4 \Psi_0^2(y) \end{aligned} \quad (71)$$

Here \mathcal{M}_3 and \mathcal{M}_4 are centered moments computed from the three-component Gaussian mixture Ψ_0^2 according to formulas in Appendix D:

$$\int dy y^3 \Psi_0^2(y) = \sum_{k=1}^3 \omega_k (\mu_k^3 + 3\mu_k \sigma_k^2), \quad \int dy y^4 \Psi_0^2(y) = \sum_{k=1}^3 \omega_k (\mu_k^4 + 6\mu_k^2 \sigma_k^2 + 3\sigma_k^4) \quad (72)$$

Equations.(71) are applicable as long as corrections $\sim b_t$ are smaller than the first terms in these formulae. Interestingly, the model predicts that a time-dependent correction to the n -th moment of a stationary distribution is approximately proportional to the $(n+1)$ -th moment, where the coefficient of proportionality has the same time dependence for all moments. This observation could shed some light on some open questions in financial modeling. In particular, [22] suggests that risk premia in equity returns are in fact premia for the skewness, rather than variance of returns. This goes contrary to the traditional financial theory such as CAPM [29] that claims that risk premia are premia for the variance. Our Eqs.(71) show that the variance and skewness of a stationary distribution are mixed in a time-dependent way in a non-equilibrium, pre-asymptotic distribution, thus suggesting that both views may be partially correct, and be in fact parts of the same time-dependent analysis. A more detailed look into implications for risk premia is left here for a future research.

4.2 Non-equilibrium option pricing and non-equilibrium dividends

In addition to providing explicit formulae for time-dependent moments of returns, the analytical approach of this paper can also be applied to option pricing in a non-equilibrium, pre-asymptotic setting. To this end, we use the simplified form (70) of a finite horizon transition density. To use it for option pricing, recall that y_t is defined as a time- t log-return computed over T years:

$$y_t = \log \frac{S_t}{S_{t-T}} \quad (73)$$

so that $y_T = \log S_T/S_0$. Above, we defined model parameters μ_k, σ_k relative to the time window T (or equivalently assuming that $T = 1$). To switch to a more conventional parameterization, we rescale means and variances $\mu_k \rightarrow \mu_k T$ and $\sigma_k^2 \rightarrow \sigma_k^2 T$, where now μ_k and σ_k are understood as annualized parameters. The transition density for y_T can then be written as follows (here we write $b = b_T$ to lighten the notation):

$$p(y_T|y_0) = C e^{b y_T} \sum_{k=1}^3 \omega_k \phi(y_T | \mu_k T, \hat{\sigma}_k^2 T), \quad \hat{\sigma}_k^2 = \frac{\sigma_k^2}{2}, \quad b = \frac{y_0}{\sigma_M} e^{-\lambda T} \quad (74)$$

where C is a normalization constant. Eq.(74) approximates pre-asymptotic effects in the time- T distribution of log-return y_T , where such effects are controlled by the time-dependent parameter b_T . The stationary distribution can formally be obtained from this expression by taking the limit $b_T \rightarrow 0$.

The non-equilibrium density (74) refers to a statistical (real-world) measure. Distributions needed for option pricing are risk-neutral distributions where by definition the expected return of any stock is given by a risk-free rate r_f . A simple approach to construct a risk-neutralized distribution $q(y_T)$ starting with a real-measure distribution $p(y_T)$ is to apply the Minimum Cross Entropy method which produces an exponential tilt to converts $p(y_T)$ into $q(y_T)$:

$$q(y_T|y_0) = C' e^{\xi y_T} p(y_T|y_0) = C e^{(b+\xi)y_T} \sum_{k=1}^3 \omega_k \phi(y_T | \mu_k T, \hat{\sigma}_k^2 T) \quad (75)$$

where C' is another normalization factor that is re-absorbed into constant C in the last equation. We want to choose the parameter ξ in such a way that the expected return *computed with the equilibrium density* (i.e. when $b_T \rightarrow 0$) is equal to $r_f T$ ¹¹:

$$\int q(y_T | b_T = 0) y_T dy_T = r_f T \quad (76)$$

The risk-neutral distribution $q(y_T)$ can now be re-written as a three-component Gaussian mixture which is similar to the real-measure stationary density Ψ_0^2 (see Eq.(29)), but has different means and weights:

$$q(y_T) = \sum_{k=1}^3 \omega_k^{(q)} \phi\left(y_T | \mu_k^{(q)} T, \hat{\sigma}_k^2 T\right) \quad (77)$$

with

$$\mu_k^{(q)} = \mu_k + (b_T + \xi) \hat{\sigma}_k^2, \quad \omega_k^{(q)} = \frac{\bar{\omega}_k}{\sum_k \bar{\omega}_k}, \quad \bar{\omega}_k = \omega_k e^{(b_T + \xi) \left(\mu_k + (b_T + \xi) \frac{\hat{\sigma}_k^2}{2} \right) T} \quad (78)$$

The value of parameter ξ that transforms the real-world distribution (74) into a risk-neutral distribution is then defined as a solution to the equation

$$\sum_{k=1}^3 \omega_k^{(q)} \mu_k^{(q)} \Big|_{b_T=0} = r_f \quad (79)$$

Re-grouping terms, this equation can also be written as follows:

$$\xi = \frac{\sum_{k=1}^3 \omega_k (r_f - \mu_k) e^{\xi T \left(\mu_k + \xi \frac{\hat{\sigma}_k^2}{2} \right)}}{\sum_{k=1}^3 \omega_k \hat{\sigma}_k^2 e^{\xi T \left(\mu_k + \xi \frac{\hat{\sigma}_k^2}{2} \right)}} \quad (80)$$

that can be quickly solved by iterating, see Fig. 6 for examples of results for ξ as a function of T . The limiting behavior at $T \rightarrow 0$ and $T \rightarrow \infty$ is

$$\xi \xrightarrow{T \rightarrow 0} \frac{\sum_{k=1}^3 \omega_k (r_f - \mu_k)}{\sum_{k=1}^3 \omega_k \hat{\sigma}_k^2}, \quad \xi \xrightarrow{T \rightarrow \infty} \frac{r_f - \mu_1}{\sigma_1^2} \quad (81)$$

A real-measure return distribution is given by the same expression (77) where one should set $\xi = 0$:

$$p(y_T) = \sum_{k=1}^3 \omega_k^{(0)} \phi\left(y_T | \mu_k^{(0)} T, \hat{\sigma}_k^2 T\right) \quad (82)$$

Now consider a European call option on S_T with maturity T and strike K and a terminal payoff $(S_T - K)_+$. The option value is defined as a discounted expected value of its payoff function with respect to the risk-neutral measure (77):

$$C(K, T) = e^{-r_f T} \int_{-\infty}^{\infty} (S_0 e^{y_T} - K)_+ q(y_T) dy_T \quad (83)$$

¹¹If we instead used the full non-equilibrium distribution $q(y_T)$ with $b_T \neq 0$, parameter b_T could be re-absorbed into a redefined value of ξ , which then would miss all non-equilibrium effects that we want to track. Also note that if we kept Eq.(69) instead of (70), parameters ξ and b_T would enter the resulting model in a non-additive way.

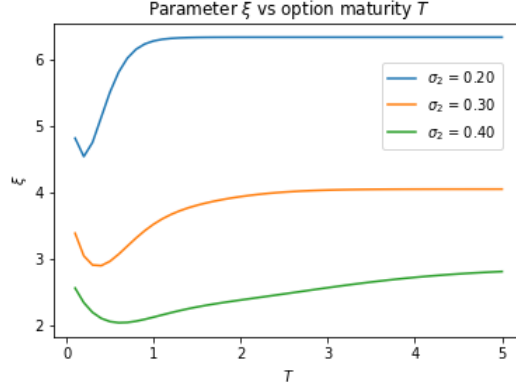


Figure 6: Profiles of parameter ξ as a function of option maturity T computed from Eq.(80). Parameters used are $\mu_1 = -\mu_2 = 0.4$, $\sigma_1 = 0.2$, $a = 0.3$, $h = 0.1$.

Plugging here Eq.(77) and performing integration, we obtain a closed-form expression for the option price in a non-equilibrium setting:

$$C(K, T) = \sum_{k=1}^3 \omega_k^{(q)} \left[S_0 e^{-q_k T} \mathcal{N}(d_1^{(k)}) - K e^{-r_f T} \mathcal{N}(d_2^{(k)}) \right] \quad (84)$$

where

$$\begin{aligned} q_k &= r_f - \mu_k - \left(\xi + b_T + \frac{1}{2} \right) \hat{\sigma}_k^2, \quad b_T = \frac{y_0}{\sigma_M} e^{-\lambda T} \\ d_1^{(k)} &= \frac{\log \frac{S_0}{K} + \left(r_f - q_k + \frac{1}{2} \hat{\sigma}_k^2 \right) T}{\hat{\sigma}_k \sqrt{T}} \\ d_2^{(k)} &= \frac{\log \frac{S_0}{K} + \left(r_f - q_k - \frac{1}{2} \hat{\sigma}_k^2 \right) T}{\hat{\sigma}_k \sqrt{T}} \end{aligned} \quad (85)$$

Each component in this sum is given by the classical Black-Scholes formula [3] for the price of a dividend-paying stock with a 'dividend' q_k . If we set here all q_k to zeros, the resulting expression coincides with a formula for a zero-dividend call option price obtained with a three-component log-normal mixture as a model of the terminal price S_T . Mixtures of lognormal price distributions, or equivalently normal mixtures for returns were previously suggested in the literature on empirical grounds as a flexible way to incorporate volatility smiles in option prices, see e.g. [2].¹² This is re-assuring, as it implies that if we treated b_T as a completely free additional model parameter, the model would be at least as good as a three-component log-normal mixture model of [2].

However, the main novelty of the non-equilibrium NES option pricing formula (84) relative to previous suggestions in the literature is exactly in the fact that the additional horizon-dependent 'dividends' q_k are *not* free parameters (and neither are the weights $\omega_k^{(q)}$). Instead, via their dependence on b_T , they are defined in terms of the original model parameters according to the way they enter the expression for the Kramers escape rate $\lambda = E_0^+ / h^2$, where the energy splitting E_0^+ is defined in Eq.(55). Because new

¹²Two-component Gaussian mixtures were also proposed for portfolio optimization in [25] as a phenomenological way to incorporate skewness of equity returns.

parameters q_k incorporate effects of non-equilibrium dynamics on option pricing, we can refer to them as effective *non-equilibrium dividends*, or NEDs for short. Once the non-equilibrium dividends q_k are estimated from calibration to option data, they can be used for scenario analyses for stocks and options.

Note that from a viewpoint of the final expressions (84) and (85), the only role of the previous machinery based on SUSY QM is to compute the Kramers escape rate λ in terms of the original model parameters, and hence to find the impact of non-equilibrium effects $\sim b_T$ on the resulting formulae for option prices or future moments of return distributions. The Kramers escape rate λ that defines parameter b_T hence also fixes the values of NEDs q_k .

Furthermore, the non-equilibrium parameter b_T also depends on the time-0 return y_0 , which means a dependence on the price S_t at time $t = -T$. While this dependence on y_0 arises as a non-equilibrium, pre-asymptotic effect in *Markov* Langevin dynamics of returns y_t , it appears as a *non-Markov* “memory” effect when translated into the price space. As suggested by the formula for b_T in Eq.(85), the impact of this term is determined by the ratio y_0/σ_M , time horizon T and the value of the Kramers escape rate λ . The NEDs q_k thus also acquire such memory effects due to their dependence on b_T .

4.3 Calibration to options: experiments with Black-Scholes options

We start with an example of model calibration for simulated data using the classical Black-Scholes setting [3]. We consider a set of $N = 10$ European call options on a zero-dividend stock with maturity $T = 1Y$, given the current price $S_0 = 50$ and its time $-T$ price of $S_{-T} = 49$. The stock volatility is $\sigma = 0.2$, and we set $r_f = 0.02$. Ten option strikes K are uniformly distributed on the interval $K = [45, 55]$. Optimization of model parameters $\theta = (\mu, \sigma_1, \sigma_2, a, h)$ is performed by minimizing the following loss function

$$\mathcal{L}(\theta) = \frac{1}{N} \sum_n \left(\frac{C_{NES}(\theta, K_n, T, S_0, y_0) - C_{BS}(K_n, \sigma, S_0)}{\Delta_{BS}(K_n, \sigma, S_0)} \right)^2 \quad (86)$$

Here the NES option prices $C_{NES}(\theta, K_n, T, S_0, y_0)$ are computed using Eq.(84), and $\Delta_{BS}(K_n, \sigma, S_0)$ is the Black-Scholes option delta. As this objective may be non-convex in parameters θ , we perform 10 calibration runs using random initial values. We use the python package *Nevergrad* version 0.4.2 [26] to perform gradient-free optimization of Eq.(86). All model parameters are constrained to lie on a unit interval, and we allow for up to 3000 function evaluations for optimization. The summary statistics for estimated model parameters are shown in Table 1, and calibrated real-measure and risk-neutralized return distributions are shown in Fig. 7.

The solutions for model parameters found by calibration to BS option prices show an interesting behavior: while calibrated real-world distributions are different for different choices of optimal parameters, the corresponding risk-neutral distributions are nearly identical, showing that local minima produce very similar values of the objective function (86). As in both the Black-Scholes model and in our formula (84) option prices are driven by risk-neutral drifts but not real-measure drifts, it appears reasonable that the real-measure drifts μ_1 and μ_2 cannot be recovered in a unique way using optimization in Eq.(86).¹³ On the other hand, different combinations of calibrated model parameters lead to numerically identical risk-neutral distributions. This implies that the latter may have certain invariances with respect to parameter transformations of the original model which is formulated in the real measure. These results are consistent with a common view that when taken in isolation, options cannot be used to uniquely identify stock returns.

¹³Recall that we set $\mu_1 = \mu$ and $\mu_2 = -\mu$ in our experiments without much loss of generality, as a non-symmetric case with different values of μ_1 and μ_2 can always be achieved by a shift of y_t .

Parameter	μ	σ_1	σ_2	a	h
mean	0.108	0.189	0.422	0.120	0.710
std	0.028	0.003	0.346	0.110	0.212
min	0.050	0.183	0.138	0.026	0.423
max	0.172	0.192	0.916	0.392	0.981

Table 1: NES parameters calibrated to Black-Scholes option prices using 10 random starting points, where all initial values are uniformly distributed between zero and 0.2.

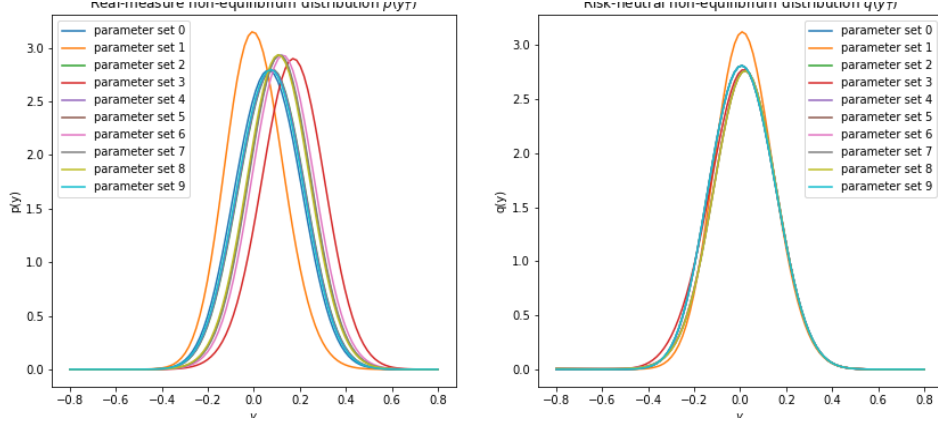


Figure 7: The left and right graphs show, respectively, the real-world and risk-neutral distributions obtained by calibration of the NES model to 10 call option prices obtained with the Black-Scholes model, for 10 different runs of optimization starting with a different initial guess. Multiple local minima lead to different real-world measures but to nearly identical risk-neutral measures.

4.4 Calibration to SPY and SPX options

Next we consider two examples of calibration to real market data. The first example deals with recent data from November 2020 for SPY options (American-type options on SPY index), while the second example deals with historical European option quotes on SPX (the S&P 500 index) from 2016. Using such different datasets enables comparing model parameters obtained for different historical periods. In addition, our second example that uses historical SPX prices enables comparing model predictions with historically observed moments of S&P 500 returns.

In the first example, we take prices of call and put options on SPY with maturity 2021/09/17 as quoted on 2020/11/06 (so that the option maturity is $T \simeq 0.86$). The underlying value of SPY on that date is 350.18. We use quoted option prices from finance.yahoo.com on the following sets of 10 strikes K that were all traded on that date: 350, 360, 365, 383, 400, 445, 475, 495, 505, 530 for calls, and 125, 140, 145, 150, 155, 185, 200, 210, 280, 350 for puts. Calibration is done separately for two sets of 10 calls and 10 puts.¹⁴ For each set, calibration is performed 10 times using randomly initialized model parameters.¹⁵ Note that a standard deviation of model parameters obtained on a single date with repeated random initializations is indicative of a variance of inferred model parameters when calibration

¹⁴This is different from most of other approaches in the literature, which typically use both sets of quotes to calls and puts simultaneously, see e.g. [9, 12], in addition to using different distributions.

¹⁵The value of a seed used in calibration is available upon request.

is performed at every time step while an initial guess for parameters is kept the same.

Calibration is performed using the same loss function as in (86), but with market quotes as targets:

$$\mathcal{L}(\theta) = \frac{1}{N} \sum_n \left(\frac{C_{NES}(\theta, K_n, T, S_0, y_0) - C_{market}(K_n, S_0)}{\Delta_{BS}(K_n, \sigma_{impl}, S_0)} \right)^2 \quad (87)$$

Here $C_{market}(K_n, S_0)$ are prices of SPY options converted to equivalent BS prices on European stocks using reported implied volatilities σ_{impl} . NES option prices $C_{NES}(\theta, K_n, T, S_0, y_0)$ are computed using Eq.(84) for call options and a corresponding relation for put options. Finally, $\Delta_{BS}(K_n, \sigma_{impl}, S_0)$ are BS deltas computed using implied volatilities σ_{impl} .

Summary statistics of calibrated model parameters are shown in Table 2, while details of individual runs can be found in Tables 8 and 9 in Appendix E. Using calibrated model parameters, we compute statistics of moments for both the real-measure and risk-neutral return distributions. Results for calibration to calls and puts are reported, respectively, in Tables 3 and 4. For both calibrations to calls and puts, both the real-world and risk-neutral distributions are negatively skewed and leptokurtic, consistently with findings in the literature, see e.g. [9]. Calibrated risk-neutral parameters and moments appear to have similar values for calibration to either calls or puts, except for a difference in volatility of about a factor of two, which is similar in the order of magnitude to differences in implied volatilities for calls and puts. When moving from the risk-neutral measure to the real one, the mean and skewness show largest differences, while other parameters show similar values across the two measures.

The resulting real-world and risk-neutral return distributions for calls and puts are shown, respectively, in Figs. 8 and 9. Potentials obtained with two sets of calibrated parameters are shown in Fig. 10. Potentials implied by puts all have a single minimum, and resemble an anharmonic oscillator potential. Such potentials produce stable dynamics. In contrast, potentials implied by the calls, while still having a single global minimum at a positive value of y , have pronounced 'butterfly' shapes with a sharp change of slope at large values of y . Some of these potentials appear to be on the brink of metastability, where a further small change is likely to produce a metastable potential similar to stylized shapes shown in Fig. 1.¹⁶

To probe variations of model calibration across different time intervals, and to compare predicted moments of returns with realized moments, in our second example we take quoted options on the SPX index on 10-03-2016 with expiry on 2017-09-27. The value of the SPX index on that date is 2162.2. Unlike options on SPY, SPX options are European, and we calibrate directly to option quotes, using option deltas as reported by OptionMetrics as weights. Proceeding similarly to the previous case of SPY options, for both calls and puts, we take 10 strikes including both an ATM strike and 9 deep OTM strikes. For the calls, we take the following strikes: 2175, 2200, 2250, 2350, 2400, 2425, 2450, 2500, 2600, 2700, and for puts, we consider strikes 750, 800, 850, 950, 1000, 1050, 1225, 1350, 1800, 2150.

Results of calibration to SPX options are reported in Table 5. Moments of real-world and risk-neutral distributions obtained for calibration to SPX calls and puts are shown, respectively, in Tables 6 and 7. Estimated moments are compared with realized moments for the period between the pricing date 10-03-2016 and options' expiries on 2017-09-27. Call and put options predict the mean returns of 0.09 and 0.07, respectively, while the realized value is 0.13. Volatility of future returns estimated from the calls is 0.01, while the realized value is 0.005. Call options appear to predict the future index volatility better than put options. On the other hand, put options appear to be better predictors of the future skewness.

¹⁶The first version of this paper found a metastable potential for call options on SPY, but these numbers were apparently based on an inconsistent set of option quotes. Nevertheless, this example can be used as an illustration that under some combinations of option quotes, a resulting potential may have two local minima and resemble some of the shapes shown in Fig. 1. During certain periods of a high market uncertainty, e.g. due to general elections, option-implied distributions can take a bimodal shape, see e.g. [12] who observed a bimodal implied distribution during British elections of 1987 (though not through other British elections in 1992), and suggested that option prices can be used as a gauge of a market sentiment during elections.

Parameter	Calibration to call options					Calibration to put options				
	μ	σ_1	σ_2	a	h	μ	σ_1	σ_2	a	h
Mean	0.09	0.13	0.42	0.55	0.21	0.13	0.36	0.999	0.28	0.47
Std	0.004	0.004	0.02	0.03	0.26	0.02	0.02	0.001	0.029	0.39
Min	0.09	0.12	0.41	0.48	0.02	0.10	0.33	0.998	0.25	0.01
Max	0.10	0.14	0.49	0.60	0.96	0.15	0.38	0.999	0.35	0.999

Table 2: NES parameters obtained by calibration to 10 call and 10 put options on SPY with expiry 2021/09/17 on 2020/11/06. Statistics of the model parameters are obtained using 10 calibration runs with a random initialization. Pricing errors for call options are between 0.1% and 1%, with a the mean of 0.7%. Pricing errors for puts are between 1% and 9%, with the mean of 4%. For details, see Tables 8 and 9 in Appendix E.

Parameter	Real measure				Risk-neutral measure			
	Mean	Std	Skewness	Kurtosis	Mean	Std	Skewness	Kurtosis
Mean	0.06	0.03	-1.08	8.39	0.01	0.04	-1.44	6.76
Std	0.007	0.003	0.08	0.81	0.001	0.005	0.12	0.51
Min	0.04	0.029	-1.23	7.26	-0.003	0.04	-1.80	5.71
Max	0.07	0.04	-1.01	10.63	0.017	0.052	-1.36	7.93
Expected	0.06	0.03	-1.03	8.25	0.017	0.04	-1.40	6.80

Table 3: Moments of the real-measure and risk-neutral distributions obtained by calibration to 10 call options on SPY with expiry 2021/09/17 on 2020/11/06. Statistics of the moments are obtained using 10 calibration runs with a random initialization. The last row called 'Expected' shows values obtained by averaging only over runs 2,3,4 that produce plausible values of the Kramers lambda, as suggested by Table 8.

Parameter	Real measure				Risk-neutral measure			
	Mean	Std	Skewness	Kurtosis	Mean	Std	Skewness	Kurtosis
Mean	0.13	0.095	-0.36	6.63	0.01	0.13	-1.41	8.77
Std	0.031	0.002	0.10	0.52	0.01	0.005	0.04	0.31
Min	0.08	0.09	-0.52	6.11	-0.002	0.12	-1.49	8.46
Max	0.17	0.10	-0.26	7.72	0.02	0.14	-1.36	9.27
Expected	0.16	0.10	-0.26	6.15	0.02	0.135	-1.37	8.47

Table 4: Moments of the real-measure and risk-neutral distributions obtained by calibration to 10 put options on SPY with maturity 2021/09/17 on 2020/11/06. Statistics of the moments are obtained using 10 calibration runs with a random initialization. The last row called 'Expected' shows values obtained by averaging only over runs 2, 5,8,9 that produce plausible values of the Kramers lambda, as suggested by Table 9.

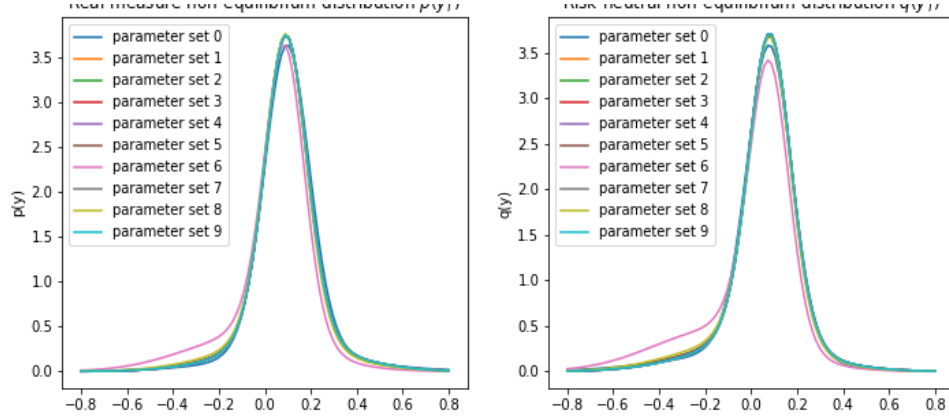


Figure 8: The left and right graphs show, respectively, the real-world and risk-neutral distributions obtained by calibration of the NES model to 10 call options on SPY with maturity 2021/09/17 on 2020/11/06, for 10 different runs of optimization with a random initialization.

This is reasonable as put options are often used to hedge downside risk, and the latter is often associated with a negative skewness.

Implied real-world and risk-neutral distributions obtained with the calls and puts are shown, respectively, in Fig. 11 and 12. Note that while the real-world distributions implied by calls are unimodal, the corresponding risk-neutral distributions are mostly bimodal. This demonstrates flexibility of our framework where, depending on the parameters, either none, or one, or both real-world and risk-neutral distributions can be bimodal.

Finally, the corresponding Langevin potentials are shown in Fig. 13. Note their similarity to potentials in Fig. 10 that were obtained by calibration to SPY options on Nov 2020. In particular, potentials implied by calls again have pronounced 'butterfly' shapes.

To summarize, comparing numbers obtained for calibrations to two different yet related datasets (SPY options on Nov 2020 vs SPX options on Oct 2016), we see that estimated model parameters have similar orders, with similar patterns for relations between risk-neutral and real-world parameters. Both calibration examples suggest that risk-neutral measures implied separately by call and put options are generally different, and have different moments.

Given that empirically implied volatilities for puts are higher than for calls, this fact should not be very surprising. Nevertheless, it conflicts with a commonly used notion of a single risk-neutral measure that applies for *both* calls and puts. When such a unique measure is taken for granted and then estimated using a joint calibration to calls and puts, any differences in distributions implied separately by calls or puts become averaged and therefore unnoticed. On the other hand, without a unique risk-neutral measure that would apply for both calls and puts, some relations such as put-call parity - that does rely on the assumption of its uniqueness - would not in general hold.

As with our approach calibration is performed for calls and puts separately, this allows one to directly compare their implied risk-neutral distributions, and see evidence that they are generally different. One possible explanation for this may be that investors in these options might have different objectives with a focus on different market scenarios. As put options are often considered as instruments for hedging tail risk, it may be natural to expect that players in this market pay more attention to crises scenarios, which should be reflected in prices of deep out of the money puts. On the other hand, a naked (unhedged) call option on SPY is essentially a bet on a future rise of the market, or equivalently a bet on good market

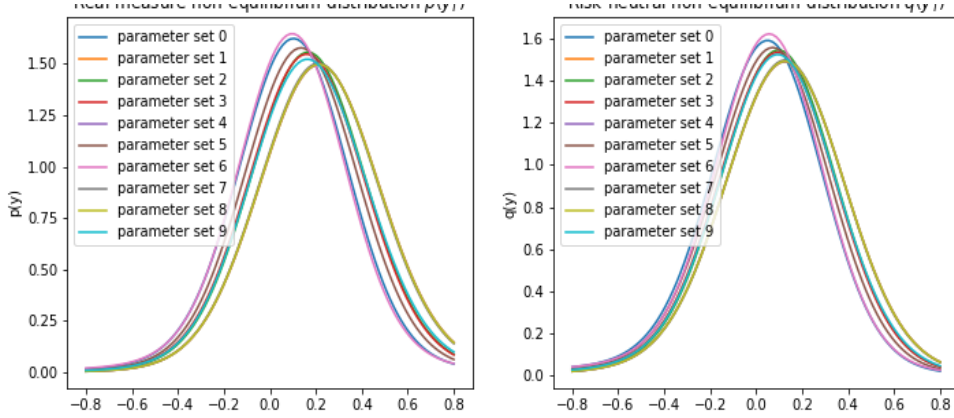


Figure 9: The left and right graphs show, respectively, the real-world and risk-neutral distributions obtained by calibration of the NES model to 10 put options on SPY with maturity 2021/09/17 on 2020/11/06, for 10 different runs of optimization with a random initialization.

Parameter	Calibration to call options					Calibration to put options				
	μ	σ_1	σ_2	a	h	μ	σ_1	σ_2	a	h
Mean	0.09	0.09	0.37	0.49	0.52	0.10	0.53	0.68	0.41	0.19
Std	0.03	0.03	0.14	0.20	0.32	0.16	0.32	0.30	0.06	0.27
Min	0.000	0.08	0.14	0.001	0.03	0.00	0.27	0.23	0.35	0.002
Max	0.101	0.15	0.75	0.87	1.00	0.58	0.99	0.91	0.50	0.92

Table 5: NES parameters obtained by calibration to 10 call and 10 put options on SPX with expiry 2017/09/27 on 2016/10/03. Statistics of the model parameters are obtained using 10 calibration runs with a random initialization. Average calibration errors for both calls and puts across different strikes are about 9%.

returns between now and option's expiry. As a result, buyers of calls and puts may have different internal models of the world, and/or use different data with their quantitative models, in deciding on the right option price. Differences in distributions implied by calls and puts may persist if they cannot be exploited by potential arbitragers due to transaction costs or other market imperfections.

4.5 Discussion

Gaussian mixtures are frequently used for modeling non-Gaussian market returns on phenomenological grounds, with an objective to fit higher moments of returns such as skewness and kurtosis, see e.g. [25]. This paper shows that with a more theoretically motivated approach, a Gaussian mixture model for returns can instead be imposed as a model of a stationary distribution, which also fixes a non-linear potential in the Langevin dynamics. With this approach, the initial two-component Gaussian mixture that defines a square root Ψ_0 of the stationary distribution in Eq.(20) is transformed into three-component Gaussian mixtures (82) and (77) for the real-world and risk-neutral measures, respectively. Unlike the former, the latter three-component mixtures capture non-stationarity by incorporating pre-asymptotic corrections to the stationary distribution Ψ_0^2 . The stationary component is parameterized in terms of parameters $\mu, \sigma_1, \sigma_2, a$. A time-varying, pre-asymptotic component of a fixed-horizon distribution of

Parameter	Real measure				Risk-neutral measure			
	Mean	Std	Skewness	Kurtosis	Mean	Std	Skewness	Kurtosis
Mean	0.08	0.01	-1.70	12.77	-0.06	0.06	-0.98	3.59
Std	0.01	0.002	0.87	5.11	0.04	0.03	0.49	0.43
Min	0.07	0.01	-2.24	3.00	-0.10	0.01	-1.38	3.15
Max	0.09	0.02	0.00	16.85	0.02	0.08	-0.01	4.42
Realized	0.13	0.005	0.09	1.81				
Expected	0.09	0.01	-1.10	10.8	-0.04	0.05	-0.60	3.31

Table 6: Moments of the real-measure and risk-neutral distributions obtained by calibration to 10 call options on SPX on 2016/10/03 with expiry 2017/09/27. Statistics of the moments are obtained using 10 calibration runs with a random initialization. Two bottom lines show realized moments estimated on data from 2016/10/03 to 2017/09/27, and the 'expected' value based on the average made only on runs 5 and 6 that produce plausible values of the Kramers escape rate, see Table 10.

Parameter	Real measure				Risk-neutral measure			
	Mean	Std	Skewness	Kurtosis	Mean	Std	Skewness	Kurtosis
Mean	0.05	0.09	0.01	8.97	0.03	0.09	-0.31	9.25
Std	0.03	0.02	0.27	1.23	0.005	0.01	0.71	1.00
Min	0.01	0.08	-0.23	7.69	0.02	0.08	-0.96	8.22
Max	0.08	0.11	0.50	10.78	0.04	0.12	0.72	10.79
Realized	0.13	0.005	0.09	1.81				
Expected	0.07	0.08	-0.07	8.19	0.03	0.09	-0.62	8.61

Table 7: Moments of the real-measure and risk-neutral distributions obtained by calibration to 10 put options on SPX on 2016/10/03 with expiry 2017/09/27. Statistics of the moments are obtained using 10 calibration runs with a random initialization. Two bottom lines show realized moments estimated on data from 2016/10/03 to 2017/09/27, and the 'expected' value based on the average made only on runs 1,2,3,4, 6 that produce plausible values of the Kramers escape rate, see Table 11.

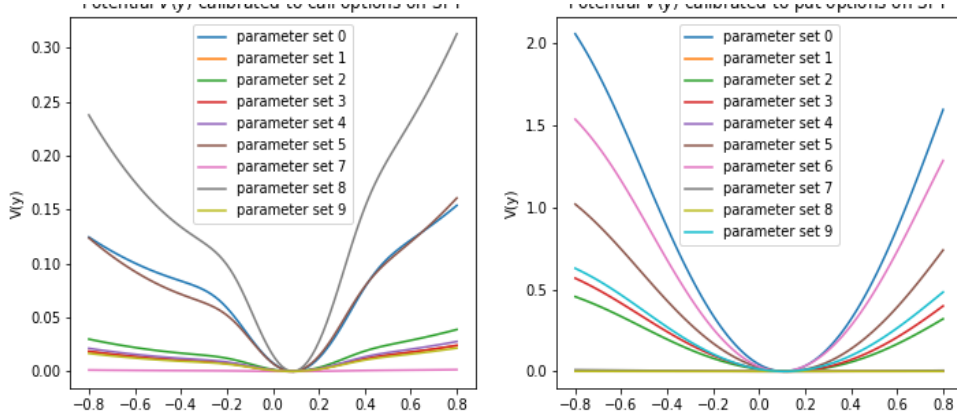


Figure 10: The LGM Langevin potentials Eq.(23) obtained by calibration of the NES model to 10 call (the graph on the left) and 10 put options (the graph on the right) on SPY with maturity 2021/09/17 on 2020/11/06, for 10 different runs of optimization starting with a different initial guess. Flat or nearly flat potential shapes are obtained with bad local minima that produce unrealistically high values of implied Kramers escape rate, defined as a rate of a large drop of returns to the level $\mu_2 = -\mu$. While potentials implied by puts remind anharmonic potentials, potentials implied by calls have pronounced 'butterfly' shapes.

market returns, is additionally driven by the volatility parameter h . As a result, moments of the return distributions such as skewness or variance acquire a time-dependent component.

Experiments show that the model is flexible and can accommodate a negative skewness and positive excess kurtosis of both real-measure and risk-neutral return distributions, and be able to extract both distributions by calibration to prices of put and call options on the SPX or SPY market indexes. The NES model is also able to smoothly shift between stable dynamics with a single minimum, and metastable dynamics obtained when the potential has two local minima separated by a barrier. As illustrated in Fig. 2, the model can adapt to different values of skewness and kurtosis of market returns.

A particularly interesting observation is that when analyzed separately and not jointly as is done in most of related research in the literature, market quotes on the call and put options seem to tell different stories about future market dynamics by producing generally different distributions. As was mentioned above, this may be explained by a market segmentation between option buyers for calls and puts, and their reliance on possibly different quantitative or internal (mental) models of the world.

This begs a practical question of what type of option data (calls or puts) is better for predicting future moments of returns. The calibration example presented above suggests that calls are better for predictions of expected returns and volatilities, while puts are better for predicting the skewness, however further numerical tests would be needed to answer this question more definitively.

Another important point is related to the fact that the least squares loss functions such as (87) typically produce multiple candidate solutions as local minima. A model parameter space may also have hyperplanes with a constant (or approximately constant) loss value, which are sometimes referred in physics as *valleys*. Note that multiple local minima (and valleys) are typically present in most of non-linear models, including in particular neural networks. However, their impact on model predictions and uncertainties around them may be altogether overlooked if all results are reported using only one fixed random seed to initialize the network for training, without trying different initializations.

In our model, we also end up with a few candidate solutions for model parameters when calibrating

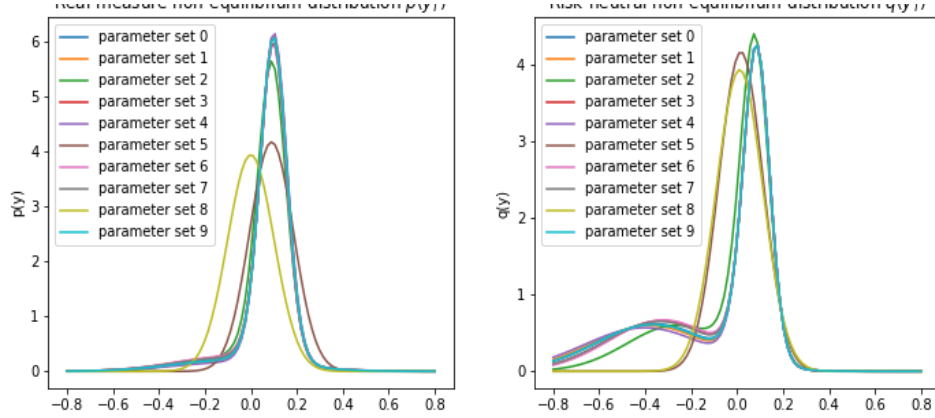


Figure 11: The left and right graphs show, respectively, the real-world and risk-neutral distributions obtained by calibration of the NES model to 10 call options on SPX with maturity 2017/09/27 on 2016/10/03, for 10 different runs of optimization with a random initialization.

separately to either calls or puts. A practical question that needs to be answered is what set or sets of calibrated parameters should be used to produce final model predictions such as moments of future returns, or crash or crisis probabilities. Our calibration results suggest that some candidate combinations of model parameters may produce reasonably looking pricing errors and moments, and yet result in a way too flat potentials that imply unrealistic escape rates. Such solutions should be rejected as they violate assumptions used in the derivation of the model.

In our experiments with 10 random initializations, we found that for calls, only runs 2,3 and 4 produce plausible values of Kramers escape rate, while for the puts, runs 2,5,8,9 produced reasonable escape rates. Averaging these numbers, we can come up with the final estimates for the Kramers escape rate λ implied by options, which gives estimates $\lambda = 557 \pm 130bp$ for calls, and $\lambda = 48 \pm 41bp$ for puts. The calls and puts thus seem to imply different probabilities of large and rare events. Such observations can be used for filtering different candidate solutions obtained by calibration to option prices.

This brings up an interesting question whether market quotes of credit indexes such as CDX or iTraxx can be used in order to improve an option based forecast on market returns. Experiments with calibration of the QED model with a similar non-linear potential in [16] demonstrated that it could be jointly calibrated to equity returns and CDS quotes. As market quotes on the CDX credit index are sometimes viewed as a proxy to a market sentiment on a next market crisis, exploring joint calibration to SPY options and CDX spreads could be an interesting extension of the analysis of this paper.

5 Summary and outlook

McCauley in his insightful and provocative book [27] pointed out various problems with traditional equilibrium approaches of classical financial models such as e.g. the CAPM model [29] or the Black-Scholes model [3]. In particular, he argued that fat tails in financial data, which is a matter of everyday concerns of practitioners and academics alike, may be simply the result of applying an unjustified binning process to non-stationary data. McCauley argued against a neoclassical economic doctrine based on the concept of a market-clearing equilibrium, and showed that among about five different definitions of a market equilibrium commonly used in the mathematical financial modeling literature, none makes sense from the physics' perspective (see also [17] for related arguments). He also issued a challenge to

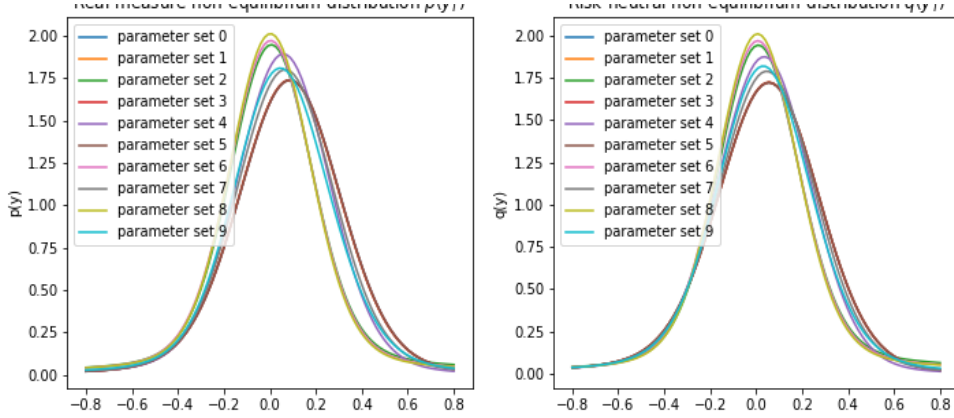


Figure 12: The left and right graphs show, respectively, the real-world and risk-neutral distributions obtained by calibration of the NES model to 10 put options on SPX with maturity 2017/09/27 on 2016/10/03, for 10 different runs of optimization with a random initialization.

econophysics as an emerging rival of the classical finance, where research often explicitly or implicitly assumes an equilibrium, potentially suffering from the same problem of a potential data distortion leading to the above-mentioned problem with problematically measured fat tails.

The Non-Equilibrium Skew (NES) model developed in this paper, as suggested by its name, provides a principled non-equilibrium view of market dynamics. It follows well defined definitions of equilibrium versus non-equilibrium dynamics as commonly accepted in the physics and applied mathematics literature. Equilibrium Langevin dynamics are obtained when a corresponding Langevin potential $V(y)$ has a single stable minimum. Metastable or unstable dynamics are obtained if the potential $V(y)$ has multiple minima. Using a two-component Gaussian mixture as the model of a ground state of a quantum mechanical system with a double well potential, we applied methods developed in supersymmetric quantum mechanics (SUSY QM) to find an analytical solution for non-equilibrium, pre-stationary dynamics.

As non-linear models rarely admit analytical solutions, they usually have much higher computational costs, which is often viewed as a main obstacle preventing their wider adaptation by practitioners. Therefore, availability of an analytical solution for non-linear non-equilibrium market dynamics may be considered a highly desirable property of a model.

Even though the first, SUSY QM-based formulation of the model *is* already analytically tractable, upon further simplifications, we produced a more practical version of the NES model based on insights derived from the previous analysis. The analytical approach further reduces the computational complexity to a very affordable mixture of three Gaussian distributions, where all parameters are fixed in terms of the original five parameters of the model. The amount of non-stationarity is directly encoded in these Gaussian mixture parameters, and thus can be directly estimated from the model fit to available data, assuming that a data-generating distribution is a non-equilibrium distribution. Note that while we only constructed the leading pre-asymptotic corrections to a stationary distribution, higher-order corrections can be computed along the same lines.

To develop a forward-looking way of model estimation, we transformed our resulting Gaussian mixture return distribution into a pricing (risk-neutral) measure, and derived closed-form expressions for prices of index (or stock) options within the NES model. The resulting formulae are given by three-component mixtures of the classical Black-Scholes expressions with different parameters. Again, all parameters in the resulting NES option pricing formula are fixed in terms of the original five model

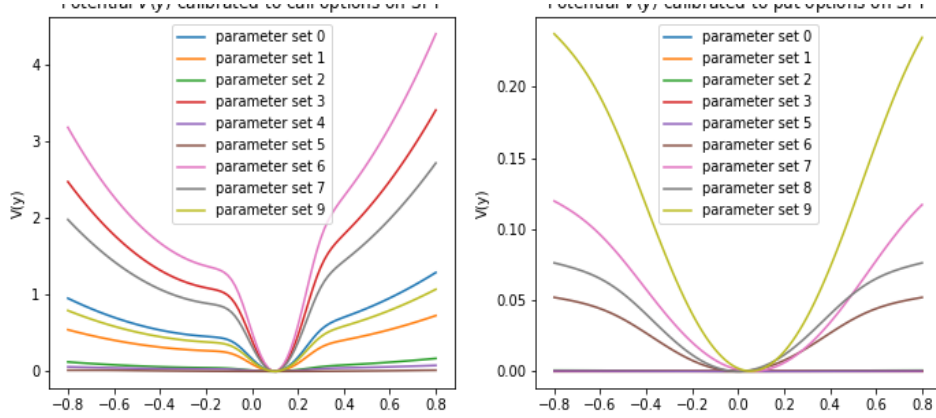


Figure 13: The LGM Langevin potentials Eq.(23) obtained by calibration of the NES model to 10 call (the graph on the left) and 10 put options (the graph on the right) on SPX with maturity 2017/09/27 on 2016/10/03 , for 10 different runs of optimization starting with a different initial guess.

parameters $\mu, \sigma_1, \sigma_2, a$ and h . All effects of non-equilibrium are mapped onto effective Non-Equilibrium Dividends (NEDs). Computational complexity of the NES model for applications to option pricing is therefore nearly on par with (three times more than) the complexity of the Black-Scholes model - however with all benefits of keeping a principled non-equilibrium approach. With this approach, the question whether market dynamics observed in different regimes can be considered as approximately equilibrium can be answered in a quantitative way.

The model developed in this paper can be used and extended in a number of interesting ways. In particular, initial numerical experiments suggest that risk-neutral measures separately implied by calls or put options are typically different, contrary to the traditional lore of the mathematical finance literature. The latter typically takes the existence of a unique risk-neutral measure for granted, and then estimates it in empirical research by a joint calibration to both calls and puts, making its approach somewhat circular. Exploring optimal combinations of information inferred separately from call and put options, and possibly incorporating new signals, e.g. credit indexes such as CDX could be an interesting future direction. Another potential direction would be to analyze applications of this framework to individual stocks, rather than to a market index. While formulas derived in this paper could also be formally applied to individual stocks, their individual dynamics should be consistent with the dynamics of the market as a whole. Such extensions are left here for a future research.

Appendix A: Instantons in the Langevin dynamics

In this appendix, we provide the explicit form of the instanton of the Langevin equation (2)

$$dy_t = -\frac{\partial V(y_t)}{\partial y_t} dt + \sigma dW_t \quad (\text{A.1})$$

using a simple cubic potential

$$V(y_t) = -\theta y_t + \frac{\kappa}{2} y_t^2 + \frac{g}{3} y_t^3 \quad (\text{A.2})$$

This potential is chosen to demonstrate a general behavior of instanton solutions in non-linear models. The potential (A.2) is different from our original potential (23), as the latter has two local minima, while the former has only one metastable minimum. On the other hand, the potential (A.2) captures the presence of a barrier for a particle located near a local minimum of a potential. For potentials with metastability such as (A.2), instantons are defined in a similar way to instantons in models with bistable potentials such as (23), as solutions corresponding to a tunneling to the ‘other side’ of the potential via tunneling to an equipotential point with the same energy, but *without* a subsequent relaxation to a second, globally stable vacuum of the theory. In quantum field theory, such solutions in metastable models without a subsequent relaxation to a stable minimum are sometimes referred to as *bounces* [7]. Though instantons in our main model with the potential (23) do not have an explicit solution of terms of elementary functions, they behave in a similar way to an instanton solution for the model (A.2) to be presented below. The only difference between them is that the end point of an instanton trajectory for the former is a global minimum of the bistable potential (23), while for the latter it is an equipotential point of the local minimum in the metastable model (A.2).

We assume that all parameters are time-independent. As discussed in [16], instantons are solutions satisfying the classical limit of the Langevin equation, but with an *inverted* sign of the potential $V(\rho)$:

$$\frac{dy_t}{dt} = \frac{dV(y_t)}{dy_t} = -\theta + \kappa y_t + g y_t^2 \quad (\text{A.3})$$

With the cubic potential (A.2), its derivative appearing in the right hand side of Eq.(A.3) is a second order polynomial. It has two roots, one corresponding to a local minimum, and another corresponding to a maximum. We denote the local minimum and maximum positions as y_\star and y^\star , respectively. A *reflection point* \hat{y} is a position on the other side of the barrier that matches the value $V(y_\star)$ at the local minimum, so that the values y_\star and \hat{y} are equipotential points. In classical mechanics, a motion between two equipotential points can proceed with vanishing kinetic energy, i.e. infinitely slow.

The instanton solution for the potential (A.2) can be found by directly integrating Eq.(A.3):

$$y_t = y_\star + \frac{\hat{y} - y_\star}{1 + e^{-g(y_\star - \hat{y})(t - t_c)}} \quad (\text{A.4})$$

where parameter t_c is called the instanton center. This is a shifted and re-scaled logistic law (sigmoid function) in time. The value y_0 of the instanton solution at time $t = 0$ is determined by the position t_c of the instanton center.¹⁷ In particular, if $t_c = 0$, then $y_0 = (y_\star + \hat{y})/2$. Assuming that $y_\star > \hat{y}$, the solution at $t \rightarrow -\infty$ is $\rho_{-\infty} = \rho_\star$, and as $t \rightarrow \infty$, it approaches $y_\infty = \hat{y}$. The instanton therefore starts at the minimum y_\star at $t \rightarrow -\infty$, and then climbs the potential wall all the way to the maximum y^\star , going *along* the gradient of the potential, and not against it as it would only be allowed in classical mechanics. After reaching the maximum y^\star at some time, the instanton then moves to the reflection point \hat{y} , reaching it

¹⁷This is different from conventional initial-value problems where an initial condition at time $t = 0$ is an input to the problem. For the instanton, there are only fixed initial and terminal values y_\star and \hat{y} for $t = \pm\infty$, while the value at $t = 0$ is determined by the instanton center t_c rather than being an independent input.

at time $t \rightarrow \infty$. On this part of its trajectory, the instanton moves *against* the gradient, consistently with conventional laws of mechanics. We can also consider an *anti-instanton* that lives backward in time: it starts at the reflection point \hat{y} at $t \rightarrow -\infty$ and reaches the local minimum at time $t \rightarrow \infty$.

Note that while y_\star and \hat{y} give the limiting positions at $t \rightarrow -\infty$ and $t = \infty$, the transition between them is well localized in time around the instanton center t_c .

Appendix B: SUSY

The Hamiltonian \mathcal{H}_- transforms into the partner Hamiltonian \mathcal{H}_+ if we flip the sign of the potential $V(y) \rightarrow -V(y)$. They can be paired in the following matrix-valued Hamiltonian:

$$\mathcal{H} = \begin{bmatrix} \mathcal{H}_+ & 0 \\ 0 & \mathcal{H}_- \end{bmatrix} = \begin{bmatrix} \mathcal{A}\mathcal{A}^+ & 0 \\ 0 & \mathcal{A}^+\mathcal{A} \end{bmatrix}. \quad (\text{B1})$$

This is the Hamiltonian of the Euclidean supersymmetric quantum mechanics of Witten [34]. It can also be represented in a form that involves fermion (anti-commuting) fields ψ_t, ψ_t^+ , in addition to the conventional boson (i.e., commuting) field y_t , see e.g. [21]. Alternatively, two purely boson Hamiltonians $\mathcal{H}_- = \mathcal{A}^+\mathcal{A}$ and $\mathcal{H}_+ = \mathcal{A}\mathcal{A}^+$ can be thought of as representing two different fermion sectors of the model. The potential $V(y)$ is referred to in the context of SUSY models as the superpotential. For a brief review of SUSY quantum mechanics, see e.g. [21, 8].

Instead of representation in terms of operators $\mathcal{A}, \mathcal{A}^+$, we can equivalently express the Hamiltonian (B1) in terms of supercharges

$$Q_1 = \frac{1}{\sqrt{2}} \begin{bmatrix} 0 & \mathcal{A} \\ \mathcal{A}^+ & 0 \end{bmatrix}, \quad Q_2 = \frac{i}{\sqrt{2}} \begin{bmatrix} 0 & -\mathcal{A} \\ \mathcal{A}^+ & 0 \end{bmatrix} \quad (\text{B2})$$

This gives

$$\mathcal{H} = 2Q_1^2 = 2Q_2^2 = Q_1^2 + Q_2^2. \quad (\text{B3})$$

This means that the Hamiltonian \mathcal{H} commutes with both supercharges, i.e. $[\mathcal{H}, Q_1] \equiv \mathcal{H}Q_1 - Q_1\mathcal{H} = 0$, and $[\mathcal{H}, Q_2] = 0$, therefore the supercharges Q_1, Q_2 are constants in time. Furthermore, Eq.(B3) shows that eigenvalues of both Hamiltonians \mathcal{H}_\pm are non-negative, with zero being the lowest possible eigenvalue.

Due to the factorization property (13), if Ψ_n^- is an eigenvector of \mathcal{H}_- with an eigenvalue $E_n^- > 0$ (where $n = 1, 2, \dots$), then the state $\Psi_n^+ \equiv (E_n^-)^{-1/2} \mathcal{A}\Psi_n^-$ will be an eigenstate of the SUSY partner Hamiltonian \mathcal{H}_+ with the same eigenvalue (energy) E_n^- (the factor $(E_n^-)^{-1/2}$ is introduced here for a correct normalization.) This is seen from the following transformation

$$\mathcal{H}_+\Psi_n^+ = (E_n^-)^{-1/2} \mathcal{A}\mathcal{A}^+\mathcal{A}\Psi_n^- = (E_n^-)^{-1/2} \mathcal{A}\mathcal{H}_-\Psi_n^- = (E_n^-)^{-1/2} \mathcal{A}E_n^-\Psi_n^- = E_n^-\Psi_n^+, \quad n = 1, 2, \dots,$$

which means that all eigenstates of spectra of H , except possibly for a 'vacuum' state with energy $E_0^- = 0$, should be degenerate in energy with eigenstates of the SUSY partner Hamiltonian \mathcal{H}_+ [34]. Such zero-energy ground state would be unpaired, while all higher states would be doubly degenerate between the SUSY partner Hamiltonians \mathcal{H}_\pm :

$$\begin{aligned} \mathcal{H}_-\Psi_0^- &= \mathcal{A}\Psi_0^- = 0, \quad E_0^- = 0 \\ \Psi_{n+1}^- &= (E_n^+)^{-1/2} \mathcal{A}^+\Psi_n^+, \quad \Psi_n^+ = (E_{n+1}^-)^{-1/2} \mathcal{A}\Psi_{n+1}^-, \quad n = 0, 1, \dots \\ E_{n+1}^- &= E_n^+, \quad n = 0, 1, \dots \end{aligned} \quad (\text{B4})$$

The existence or non-existence of a zero-energy ground state $E_0^- = 0$ has to do with supersymmetry being unbroken or spontaneously broken. In scenarios with spontaneous breaking of SUSY, supersymmetry is a symmetry of a Hamiltonian but not of a ground state of that Hamiltonian. On the other hand, an unbroken SUSY is characterized by the existence of a normalizable ground state Ψ_0 with strictly zero energy $E_0 = 0$, while for a spontaneously broken SUSY the energy of the ground state is larger than zero [34]:

$$\begin{aligned} \text{Unbroken SUSY:} \quad & A\Psi_0 = 0 \cdot \Psi_0 = 0 \quad (E_0 = 0) \\ \text{Spontaneously broken SUSY:} \quad & A\Psi_0 = E_0\Psi_0, \quad E_0 > 0. \end{aligned} \quad (\text{B5})$$

For SUSY to be unbroken, the derivative of the superpotential $V'(y) = \partial V / \partial y$ should have different signs at $y = \pm\infty$, which means that it should have an odd number of zeros at real values of y .

Appendix C: Logarithmic Perturbation Theory

This appendix presents Logarithmic Perturbation Theory (LPT) for a ground state wave function and energy for a one-dimensional Schrödinger equation. Further details can be found in [1, 32].

We consider the following Schrödinger equation with $m = 1$:

$$\left[-\frac{\hbar^2}{2} \frac{\partial^2}{\partial x^2} + V_0(x) + \alpha V_1(x) \right] \psi(x) = E\psi(x) \quad (\text{C.1})$$

where parameter α is assumed to be small, and we are only interested in the lowest energy eigenstate. As the ground state function is nodeless, we look for a solution in the form

$$\psi(x) = \exp \left[-\frac{G(x)}{\hbar} \right] \quad (\text{C.2})$$

where a function $G(x)$ is assumed to be twice differentiable. Substituting (C.2) into (C.1), we obtain the Riccati equation for the derivative $g(x) = G'(x)$:

$$\frac{1}{2}g^2(x) - \frac{\hbar}{2}g'(x) + E - V_0(x) - \alpha V_1(x) = 0 \quad (\text{C.3})$$

We can solve this equation in terms of perturbative series for $g(x)$ and E :

$$g(x) = \sum_{k=0}^{\infty} \alpha^k g_k(x), \quad E = \sum_{k=0}^{\infty} \alpha^k \bar{E}_k \quad (\text{C.4})$$

Note that here k enumerates the perturbative order of the calculation, and not the energy level. As we are only interested here in the lowest energy eigenstate, we do not need a subscript labeling different eigenstates. Using (C.4) in (C.3) and comparing coefficients for various powers of α , we find

$$\begin{aligned} \frac{1}{2}g_0^2 - \frac{\hbar}{2}g_0' &= V_0 - \bar{E}_0 \\ g_0g_1 - \frac{\hbar}{2}g_1' &= V_1 - \bar{E}_1 \\ 2g_0g_k - \hbar g_k' &= \sum_{j=1}^{k-1} g_jg_{k-j} - \bar{E}_k, \quad k \geq 2 \end{aligned} \quad (\text{C.5})$$

The first equation here is just the Schrödinger equation for the unperturbed problem with the ground-state WF $\psi_0(x)$, expressed in terms of $g_0(x)$. Multiplying the second equation by the integrating factor $\exp(-2G_0(x)/\hbar) = \psi_0^2(x)$, we obtain

$$\frac{d}{dx} \left(g_1(x) \psi_0^2(x) \right) = -\frac{2}{\hbar} (V_1(x) - \bar{E}_1) \psi_0^2(x) \quad (\text{C.6})$$

Integrating this equation from $-\infty$ to ∞ and using the fact that $\psi_0(x)$ satisfies the zero boundary conditions at $x = \pm\infty$, we find the first order correction to the energy:

$$\bar{E}_1 = \frac{\int_{-\infty}^{\infty} dz V_1(z) \psi_0^2(z)}{\int_{-\infty}^{\infty} dz \psi_0^2(z)} \quad (\text{C.7})$$

Now when E_1 is specified, Eq.(C.6) can be integrated from $-\infty$ to x for $x > 0$, or from x to ∞ for $x < 0$, producing the following result yields

$$g_1(x) = \begin{cases} \frac{2}{\hbar} \frac{1}{\psi_0^2(x)} \int_{-\infty}^x dz (\bar{E}_1 - V_1(z)) \psi_0^2(z), & x > 0 \\ -\frac{2}{\hbar} \frac{1}{\psi_0^2(x)} \int_x^{\infty} dz (\bar{E}_1 - V_1(z)) \psi_0^2(z), & x < 0 \end{cases} \quad (\text{C.8})$$

Using this expression, we obtain the first order correction to the wave function:

$$G_1(x) = \begin{cases} \frac{2}{\hbar} \int_{-\infty}^x dy \frac{1}{\psi_0^2(y)} \int_{-\infty}^y dz (\bar{E}_1 - V_1(z)) \psi_0^2(z) + C, & x > 0 \\ -\frac{2}{\hbar} \int_{-\infty}^x dy \frac{1}{\psi_0^2(y)} \int_y^{\infty} dz (\bar{E}_1 - V_1(z)) \psi_0^2(z) + C, & x < 0 \end{cases} \quad (\text{C.9})$$

Here C is a constant that should be fixed from a normalization condition on a perturbed wave function. Note that the integrand in this expression is non-singular at $y \rightarrow \infty$ due to Eq.(C.7).

We can further introduce the “effective potential” which is calculated recursively at each given order in λ :

$$V_i^{eff}(x) = \sum_{j=1}^{i-1} g_j(x) g_{i-j}(x), \quad i \geq 2 \quad (\text{C.10})$$

Performing the same manipulations as above with the last of Eqs.(C.5), we obtain

$$\bar{E}_i = \frac{\int_{-1}^1 dz V_i^{eff}(z) \psi_0^2(z)}{\int_{-1}^1 dz \psi_0^2(z)}$$

$$g_i(x) = \frac{1}{\hbar \psi_0^2(x)} \int_{-1}^x dz \left[\bar{E}_i - V_i^{eff}(z) \right] \psi_0^2(z) \quad (\text{C.11})$$

$$G_i(x) = \frac{1}{\hbar} \int_{-1}^x dy \frac{1}{\psi_0^2(y)} \int_{-1}^y dz \left[\bar{E}_i - V_i^{eff}(z) \right] \psi_0^2(z) + C_i \quad (\text{C.12})$$

Equations (C.7)-(C.11) provide a recursive scheme by which perturbative corrections to the energies and wave functions can be calculated to any order in the coupling λ . In contrast to the standard Rayleigh-Schrödinger (RS) perturbation theory, they do not require a calculation of matrix elements of the perturbation potential V_1 . While the new scheme can be shown to be equivalent to the RS perturbation theory [1], it is far more convenient for calculating perturbative corrections due to its quadrature, recursive form.

Appendix D: Higher moments of Gaussian mixtures

Consider a random real-valued variable X whose probability density function (pdf) of realizations $X = x$ is given by a Gaussian mixture

$$f_{\theta}(x) = \sum_{k=1}^K \omega_k \phi(x|\mu_k, \sigma_k^2), \quad \sum_{k=1}^K \omega_k = 1, \quad 0 \leq \omega_k \leq 1 \quad (\text{D1})$$

Here θ stands the vector of all parameters (μ_k, σ_k^2) of K Gaussian components, with $\phi(x|\mu_k, \sigma_k^2)$ being the Gaussian pdfs with the means μ_k and variances σ_k^2 . The moment generating function (MGF) is defined as follows:

$$M(z) := \mathbb{E} [e^{zX}] = \sum_{k=1}^K \omega_k \mathbb{E}_k [e^{zX}] = \sum_{k=1}^K \omega_k \exp \left[\mu_k z + \frac{\sigma_k^2}{2} z^2 \right] \quad (\text{D2})$$

where $\mathbb{E}_k [\cdot]$ stands for an expected value computed using the k -th component of the Gaussian mixture (D1). All moments M_n can be conveniently computed from the MGF (D2) as coefficients of its Taylor expansion around $z = 0$:

$$M(z) = \sum_{n=0}^{\infty} \frac{M_n}{n!} z^n \quad (\text{D3})$$

This gives uncentered moments

$$\begin{aligned} \hat{\mu} := M_1 = \mathbb{E} [X] &= \sum_{k=1}^K \omega_k \mu_k, \quad M_2 = \mathbb{E} [X^2] = \sum_{k=1}^K \omega_k (\mu_k^2 + \sigma_k^2), \\ M_3 = \mathbb{E} [X^3] &= \sum_{k=1}^K \omega_k (\mu_k^3 + 3\mu_k \sigma_k^2), \quad M_4 = \mathbb{E} [X^4] = \sum_{k=1}^K \omega_k (\mu_k^4 + 6\mu_k^2 \sigma_k^2 + 3\sigma_k^4) \end{aligned} \quad (\text{D4})$$

Centered moments can be computed using (D4). In particular, for the variance of the mixture we obtain

$$\hat{\sigma}^2 := \mathbb{E} [X^2] - (\mathbb{E} [X])^2 = \sum_{k=1}^K \omega_k \left(\mu_k^2 + \sigma_k^2 - \mu_k \sum_{k'} \omega_{k'} \mu_{k'} \right) \quad (\text{D5})$$

The skewness is a normalized centered third moment

$$\tilde{\mu}_3 := \mathbb{E} \left[\left(\frac{X - \hat{\mu}}{\hat{\sigma}} \right)^3 \right] = \frac{\mathbb{E} [(X - \hat{\mu})^3]}{(\mathbb{E} [(X - \hat{\mu})^2])^{3/2}} = \frac{\mathbb{E} [X^3] - 3\hat{\mu} \mathbb{E} [X^2] + 2\hat{\mu}^3}{\hat{\sigma}^3} \quad (\text{D6})$$

The kurtosis is the normalized centered fourth moment

$$\tilde{\mu}_4 := \mathbb{E} \left[\left(\frac{X - \hat{\mu}}{\hat{\sigma}} \right)^4 \right] = \frac{\mathbb{E} [(X - \hat{\mu})^4]}{(\mathbb{E} [(X - \hat{\mu})^2])^2} = \frac{\mathbb{E} [X^4] - 4\hat{\mu} \mathbb{E} [X^3] + 6\hat{\mu}^2 \mathbb{E} [X^2] - 3\hat{\mu}^4}{\hat{\sigma}^4} \quad (\text{D7})$$

Appendix E: Details of calibration experiments

Run	μ	σ_1	σ_2	a	h	Mean pricing error	Kramers lambda
1	0.093	0.139	0.493	0.484	0.220	0.001	0.277
2	0.088	0.127	0.415	0.550	0.082	0.001	0.046
3	0.088	0.127	0.415	0.551	0.104	0.001	0.074
4	0.088	0.127	0.415	0.550	0.082	0.003	0.047
5	0.088	0.127	0.415	0.550	0.088	0.008	0.053
6	0.090	0.128	0.424	0.549	0.214	0.010	0.299
7	0.100	0.120	0.417	0.597	0.957	0.015	4.681
8	0.087	0.128	0.415	0.548	0.021	0.012	0.003
9	0.092	0.125	0.417	0.566	0.297	0.010	0.549
10	0.088	0.128	0.415	0.550	0.078	0.011	0.042

Table 8: Results of parameter calibration to SPY calls on 2020-11-06 obtained on 10 runs with a random initialization, where all initial values are uniformly distributed between zero and 0.2. The last column is the escape rate to reach the value $\mu_2 = -\mu$.

Run	μ	σ_1	σ_2	a	h	Mean pricing error	Kramers lambda
1	0.110	0.345	1.000	0.297	0.999	0.071	3.715
2	0.155	0.380	1.000	0.252	0.016	0.011	0.001
3	0.132	0.362	1.000	0.281	0.474	0.021	0.673
4	0.131	0.364	0.998	0.280	0.531	0.022	0.850
5	0.155	0.380	1.000	0.253	0.051	0.039	0.006
6	0.122	0.357	1.000	0.279	0.705	0.040	1.631
7	0.099	0.332	1.000	0.346	0.883	0.007	3.217
8	0.153	0.378	1.000	0.258	0.066	0.046	0.011
9	0.154	0.380	1.000	0.254	0.015	0.056	0.001
10	0.107	0.340	1.000	0.309	0.998	0.090	3.832

Table 9: Results of parameter calibration to SPY puts on 2020-11-06 obtained on 10 runs with a random initialization, where all initial values are uniformly distributed between zero and 0.2. The last column is the escape rate to reach the value $\mu_2 = -\mu$.

Run	μ	σ_1	σ_2	a	h	Mean pricing error	Kramers lambda
1	0.101	0.077	0.357	0.501	0.514	0.10	0.61
2	0.101	0.078	0.366	0.494	0.390	0.10	0.34
3	0.093	0.083	0.307	0.492	0.171	0.11	0.11
4	0.101	0.077	0.339	0.516	0.814	0.11	1.66
5	0.101	0.078	0.378	0.483	0.129	0.10	0.04
6	0.086	0.137	0.751	0.000	0.034	0.09	0.009
7	0.101	0.076	0.335	0.520	0.920	0.09	2.17
8	0.101	0.077	0.343	0.513	0.731	0.10	1.32
9	0.000	0.153	0.144	0.874	1.000	0.16	5.34
10	0.101	0.077	0.359	0.499	0.469	0.15	0.51

Table 10: Results of parameter calibration to SPX calls obtained on 10 runs with a random initialization, where all initial values are uniformly distributed between zero and 0.2. The last column is the escape rate to reach the value $\mu_2 = -\mu$.

Run	μ	σ_1	σ_2	a	h	Mean pricing error	Kramers lambda
1	0.079	0.294	0.891	0.352	0.003	0.18	5.7e-5
2	0.078	0.293	0.894	0.356	0.003	0.05	6.3e-5
3	0.000	0.999	0.232	0.467	0.019	0.04	8.3e-3
4	0.079	0.293	0.892	0.354	0.003	0.10	4.4e-5
5	0.061	0.270	0.866	0.352	0.917	0.13	6.75
6	0.079	0.294	0.891	0.353	0.011	0.13	7.7e-4
7	0.000	0.999	0.234	0.489	0.164	0.08	0.61
8	0.063	0.280	0.907	0.381	0.238	0.02	0.43
9	0.000	0.996	0.231	0.491	0.198	0.04	0.91
10	0.577	0.565	0.807	0.502	0.327	0.13	0.035

Table 11: Results of parameter calibration to SPX puts obtained on 10 runs with a random initialization, where all initial values are uniformly distributed between zero and 0.2. The last column is the escape rate to reach the value $\mu_2 = -\mu$.

References

- [1] Y. Aharonov and C.K. Au, "New Approach to Perturbation Theory", *Phys. Rev. Lett.* **42** (1979) 1582.
- [2] C. Alexander and S. Narayanan, "Option Pricing with Normal Mixture Returns: Modelling Excess Kurtosis and Uncertainty in Volatility", ICMA Centre Discussion Papers in Finance icma-dp2001-10, Henley Business School, Reading University (2001).
- [3] F. Black and M. Scholes, "The Pricing of Options and Corporate Liabilities", *Journal of Political Economy*, Vol. 81(3), 637-654, 1973.
- [4] J.P. Bouchaud and R. Cont, "A Langevin Approach To Stock Market", *The European Physical Journal B*, **6**(4), 543-550 (1998).
- [5] M. Bernstein and L.S. Brown, "Supersymmetry and the Bistable Fokker-Planck Equation", *Physical Review Letters*, **52** (22), 1933-1935 (1984).
- [6] F. Chabi-Yo, D. Liesen, and E. Renault, "Implications of Asymmetry Risk for Portfolio Analysis and Asset Pricing", Bank of Canada (2007).
- [7] S. Coleman, *Aspects of Symmetry. Selected Erice Lectures*, Cambridge University Press (1988).
- [8] F. Cooper, A. Khare, and I. Sukhatme, *Supersymmetry in Quantum Mechanics*, World Scientific (2001).
- [9] C.J. Corrado and T. Su, "Implied volatility skews and stock index skewness and kurtosis implied by S&P 500 index option prices", *Journal of Derivatives* 5, 8-19 (1996).
- [10] A. Gangopadhyaya, P.K. Panigrahi, and U.P. Sukhatme, "Supersymmetry and Tunneling in an Asymmetric Double Well", *Phys. Rev. A*, vol. 47 (no. 4), 2720-2724 (1993).
- [11] Gardiner, *Handbook of Stochastic Methods*, Springer (1996).
- [12] G. Gemmill and A. Saflekos, "How Useful are Implied Distributions? Evidence from Stock-Index Options" (2000), *The Journal of Derivatives*, 7 (3), 83-91 (2000), available at <https://www.bis.org/publ/bisp06e.pdf>.
- [13] M.V. Feigelman and A.M. Tsvelik, "Hidden Supersymmetry of Stochastic Dissipative Dynamics", *Sov. Phys. JEPT*, **56** (4), 823-830 (1982).
- [14] T.R.T. Ferreira, "Stock Market Cross-Sectional Skewness and Business Cycle Fluctuations", Board of Governors of the Federal Reserve System, <https://www.federalreserve.gov/econres/ifdp/files/ifdp1223.pdf> (2018).
- [15] P. Hanggi, "Escape from a Metastable State", *Journal of Statistical Physics*, **42** (1/2) 105-148 (1986).
- [16] I. Halperin and M.F. Dixon, "Quantum Equilibrium-Disequilibrium: Asset Price Dynamics, Symmetry Breaking, and Defaults as Dissipative Instantons", *Physica A* **537**, 122187, <https://doi.org/10.1016/j.physa.2019.122187> (2020).
- [17] I. Halperin, "The Inverted World of Classical Quantitative Finance: a Non-Equilibrium and Non-Perturbative Finance Perspective", <https://arxiv.org/abs/2008.03623> (2020).

- [18] I. Halperin, “Dumb Money, The Origin of Factors, Skew and Rare Events: Interacting-assets “Quantum Equilibrium-Disequilibrium””, forthcoming (2020).
- [19] C.R. Harvey and A. Siddique, “Time-Varying Conditional Skewness and the Market Risk Premium”, *Research in Banking in Finance*, vol. 1, pp. 25-58 (2000).
- [20] W.-Y. Keung, E. Kovacs, and U. Sukhatme, “Supersymmetry and Double Well Potentials”, *Phys. Rev. Lett.* **60** (1988) 41.
- [21] G. Junker, *Supersymmetric Methods in Quantum and Statistical Physics*, Springer 1996.
- [22] Y. Lempérière, C. Deremble, T. T. Nguyen, P. Seager, M. Potters, J. P. Bouchaud, “ Risk Premia: Asymmetric Tail Risks and Excess Returns”, *Quantitative Finance* vol. 17, no.1, 1-14, <https://arxiv.org/abs/1409.7720> (2017).
- [23] L.D. Landau and E.M. Lifschitz, *Quantum Mechanics*, Elsevier (1980).
- [24] P. Langevin, “Sur la Théorie du Mouvement Brownien”, *Comps Rendus Acad. Sci. (Paris)* 146, 530-533 (1908).
- [25] E. Lezmi, H. Malongo, T. Roncalli, and R. Sobotka, “Portfolio Allocation with Skewness Risk: a Practical Guide”, available at <http://www.thierry-roncalli.com/download/Skewness-Risk-Allocation.pdf>.
- [26] <https://github.com/facebookresearch/nevergrad>.
- [27] McCauley, *Dynamics of Markets: The New Financial Economics*, 2nd edition, Cambridge University Press (2009).
- [28] C. Ren and A.R. MacKenzie, “Closed-Form Approximations to the Error and Complimentary Error Functions and Their Applications in Atmospheric Science”, *Atmospheric Science Letters*, v. 8, issue 3, pp.70-73 (2007), <https://rmets.onlinelibrary.wiley.com/doi/full/10.1002/asl.154>.
- [29] W.F. Sharpe, “Capital Asset Prices: A Theory of Market Equilibrium Under Conditions of Risk”, *Journal of Finance*, **19** (3), 425-442 (1964).
- [30] P.S. Stilger, A. Kostakis, and S.H. Poon, “What Does Risk-Neutral Skewness Tell Us About Future Stock Returns?”, *Management Science*, vol. 63, Issue 3, 1657-2048 (2016).
- [31] D. Sornette, *Why Stock Markets Crash*, Princeton University Press (2003).
- [32] A.V. Turbiner, “A New Approach to the Eigenvalue Problem in Quantum Mechanics: Convergent Perturbation Theory for Rising Potentials”, *JETP Lett.* **30** (1979) 352, *J.Phys.* **A14** (1981)1641.
- [33] N.G. Van Kampen, *Stochastic Processes in Physics and Chemistry*, North-Holland (1981).
- [34] E. Witten, "Dynamical Breaking of Supersymmetry", *Nuclear Physics B* **188**(3-5), 513-554 (1981).
- [35] “With four parameters I can fit an elephant, and with five I can make him wiggle his trunk.” (John von Neumann).
- [36] C. Zinn-Justin, *Quantum Field Theory and Critical Phenomena*, Fourth Edition, Clarendon Press, Oxford (2002).